

# Observer-Based Intensity-Feedback Control for Laser Beam Pointing and Tracking

Néstor O. Pérez-Arancibia, *Member, IEEE*, James S. Gibson, *Member, IEEE*, and Tsu-Chin Tsao, *Senior Member, IEEE*

**Abstract**—This paper presents an investigation of the control problem of aiming a laser beam under dynamic disturbances, using light intensity for feedback only. The idea is to steer the beam with a biaxial microelectromechanical mirror, which is driven by a control signal generated by processing the beam intensity sensed by a single photodiode. Since the pointing location of the beam is assumed to be unavailable for real-time control, a static nonlinear mapping from the 2-D beam location to the photodiode sensor measurement output is estimated with the use of the least-squares algorithm, treating data from a biaxial optical position sensor as inputs to the static mapping. This formulation results in a nonlinear Wiener–Hammerstein system composed of a linear subsystem connected in series to a nonlinear static output mapping. Conceptually, the controller design problem is addressed with the integration of an observer and a pair of linear time-invariant single-input/single-output controllers into one system. This approach motivates two research questions that are considered independently in this paper. The first is about the multiple-experiment observability of the considered nonlinear optical system. The second is about the search of an heuristic method, based on the extended Kalman filter (EKF) algorithm, for estimating the state of the linear subsystem, necessary for implementing the proposed control approach. Here, we present a compelling answer for the first question and we propose a methodology to tackle the second. It is important to state that the problem considered in this article is very challenging, because the nonlinear static output map of the system is not one-to-one. In order to address this issue, we introduce the idea of integrating stable output disturbance models into the design of the proposed EKF-based observer. This is the main contribution of the paper, which could have an impact in the way other nonlinear control problems are addressed in the future. Evidence of the suitability of the proposed method is provided through experimental results from a case relevant to free-space optics for communications and directed energy applications.

**Index Terms**—Extended Kalman filter (EKF), Gröbner bases, light-intensity feedback, nonlinear observability, Wiener-Hammerstein nonlinear systems.

## I. INTRODUCTION

**L**ASER beams are used to transmit information or energy in a wide range of applications, from laser cutting to metrology, from laser surgery to communications. Applications

Manuscript received May 31, 2010; revised November 07, 2010; accepted January 11, 2011. Manuscript received in final form January 25, 2011. Date of publication March 10, 2011; date of current version December 14, 2011. Recommended by Associate Editor A. Alessandri. This work was supported by the Office of Naval Research under Grant N00014-07-1-1063.

N. O. Pérez-Arancibia was with the Mechanical and Aerospace Engineering Department, University of California, Los Angeles, CA 90095-1597 USA. He is now with the School of Engineering and Applied Sciences, Harvard University, Cambridge, MA 02138 USA (e-mail: nperez@seas.harvard.edu; nestor\_p\_a@yahoo.com).

J. S. Gibson and T.-C. Tsao are with the Mechanical and Aerospace Engineering Department, University of California, Los Angeles, CA 90095-1597 USA (e-mail: gibson@ucla.edu; ttsao@seas.ucla.edu).

Color versions of one or more of the figures in this paper are available online at <http://ieeexplore.ieee.org>.

Digital Object Identifier 10.1109/TCST.2011.2109720

typically require the beam to aim at a target with a maximum possible light intensity level, or above a specified threshold value, traveling through free space, the atmosphere or other transmissible media, while subjected to disturbances from multiple sources. In most beam control systems, biaxial sensors, such as, optical position sensors (OPSs), charge-coupled devices (CCDs), or simple quad-photo detectors, are used to determine the coordinated location of the beam projection on a plane, which is feedback into a two-input/two-output controller (e.g., see [1]–[3] and references therein).

In many applications in which tracking is not attempted because the use of biaxial coordinate sensors is not convenient due to cost, space, or other technical reasons, single photodiode sensors are currently being used for purposes other than feedback control. Thus, the possibility of using single photodiode sensors for feedback control is of great interest, since this might significantly increase the overall performance and reliability of some common optical systems which already contain photodiode sensors. For example, in the area of free-space laser communications, laser beams are modulated at high frequencies, in order to encode and transmit data. In those systems, there are optical links that require specified minimum amounts of laser power at the receiver's end, so that, data loss is minimized during the decoding process.

A method to approach the problem, based on the notion of nutation, is presented in [4]. There, a small high-frequency nutation signal is inputted to the system, inducing a known, or estimable, additional tracking error, used for determining the spatial position of the laser beam center. If implemented in discrete-time, this method requires extremely high sampling rates. Another approach, and a matter of further research, is the implementation of some kind of real-time optimization algorithm, based on methods such as artificial neural networks [5] or extremum seeking control [6].

A third approach, the one considered here, is the implementation of an observer-based controller. This idea motivates two research lines that are explored in this work. The first focuses on the observability of the nonlinear optical system that results from replacing the optical position sensor used in [3] by a single photodiode sensor. Here, it is empirically shown that the nonlinear system can be represented by a polynomial nonlinear model that falls in the class studied in [7] and [8]. In this particular case, the whole optical path can be modeled as a Wiener-Hammerstein system, in which a linear subsystem is connected in series to a convex static mapping. Based on the ideas and methods in [8], we argue that the multiple-experiment observability of the kind of optical systems investigated here can be determined using the concept of Gröbner basis.

In the second line of research, we empirically perform experiments in the search of a heuristic method for estimating the state of the linear time-invariant (LTI) subsystem composing part of the optical nonlinear system. Specifically, we employ an extended Kalman filter (EKF) [9], [10] to estimate the bidimensional position of the laser beam center on an imaginary plane, using the intensity measurement obtained from a single photodiode sensor. Then, the estimated coordinates are used to generate a control signal by means of a pair of single-input/single-output (SISO) LTI controllers. This is reasonable, because the original control objective is to maximize the light intensity detected by the photodiode sensor, and this objective is equivalent to positioning the laser beam center at a specific position over an imaginary coordinated plane where the light intensity is maximized. It is known that the relationship between position coordinates and intensity can be approximated by quadratic static functions [4]. It is important to state that since the static convex mapping is not one-to-one, this is a very challenging estimation problem.

Here, a static mapping is estimated using the least-squares algorithm from 450 000 data samples obtained using a biaxial OPS and the photodiode sensor employed for control. The EKF is a heuristic solution, and therefore, there is no guarantee of optimality, or even, functionality. The experimental results presented here suggest that it is not possible to steer the system to the desired optimal operation point. However, we show empirically that the laser beam can be steered to suboptimal operation points, improving the overall performance of the optical system significantly, because a noticeable amount of disturbance can be rejected. This could be of great utility in many applications. For example, in laser communications, the power at the receiving end of an optical link is required to be above a specified threshold value in order to maintain the communication link. Therefore, it is more desirable that the sensor receives an amount of light above a specified value at each time instant than it is that the sensor receives a large amount of light at sporadic time instants.

The rest of the paper is organized as follows. Sections II describes the experimental setup and plants involved. Section III addresses the question of the multiple-experiment observability of the optical nonlinear open-loop system. Section IV reviews some fundamental aspects of the EKF. Section V describes the experimental implementation of the observer in open-loop, i.e., the system is excited with white noise and no control signal is generated using feedback. Section VI describes the proposed method for designing observer-based controllers and discusses the implementation of light-intensity feedback control schemes for laser beam pointing and tracking. Section VII presents experimental results, and, finally, Section VIII draws some conclusions.

#### Notation

- $\mathbb{R}$  and  $\mathbb{N}$  denote the sets of real and natural numbers, respectively.
- $\mathbb{K}$  denotes a generic number field.

## II. EXPERIMENTAL SETUP AND SYSTEM IDENTIFICATION

A scheme and a photograph of the system considered in this paper are shown in Figs. 1 and 2, respectively. There, a laser

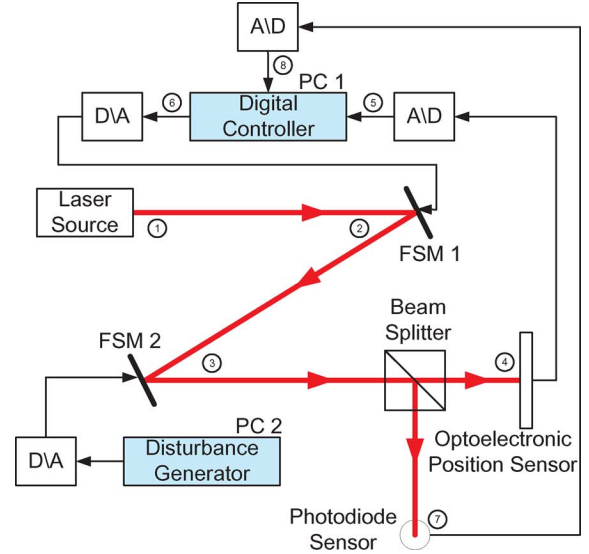


Fig. 1. Diagram of the experiment.

beam is generated with a laser source at position ①. Immediately after, the laser beam reflects off the biaxial fast steering mirror FSM 1 at position ②, then it reflects off the biaxial fast steering mirror FSM 2 at position ③ and before reaching positions ④ and ⑦ it is split using a non-polarizing beam-splitter cube. At positions ④ and ⑦, a 2-D OPS and a single photodiode sensor are located, respectively. FSM 1 and FSM 2 are identical Texas Instruments (TI) microelectromechanical MEMS mirrors used in laser communications for commercial and defense applications, and the OPS is an on-track sensing device. For further details on the sensor, refer to [2] and [3]. FSM 1 is used for control actuation and FSM 2 is used for generating jitter, which disturbs the laser beam horizontally and vertically. A second possible source of jitter is a shaker with vertical motion on which the control actuator FSM 1 is mounted.

The OPS determines the coordinates of the laser-beam spot center on the sensor, and then, these measurements, in the form of voltages, are sent to a computer, labeled as PC 1, used for control. As described in [2] and papers therein, high performance position feedback controllers, based on LTI, adaptive or other methods, can be designed and implemented using the almost-perfect coordinate location information provided by biaxial optical position sensors. In this work, OPS measurements are used for monitoring and identification purposes, but not for control. Feedback control is performed using the light intensity measurement generated by the single photodiode sensor at position ⑦, only. PC 1 runs the feedback controller that generates and sends actuator commands to FSM 1, and another computer, labeled as PC 2, sends disturbance commands to FSM 2 and to the shaker. The sampling and computing rate, to which the digital controller and the disturbance generator are run, is 5 KHz.

In the rest of this paper,  $P$  is the open-loop LTI transfer function that maps the two-channel digital control command, marked by ⑥ in Fig. 1, to the sampled two-channel position sensor output, marked by ⑤ in Fig. 1. Thus,  $P$  is the two-input/two-output digital transfer function for FSM 1 with a variable gain depending on the location of the OPS and the

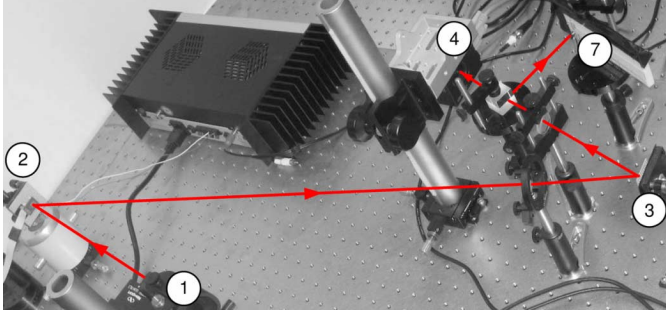


Fig. 2. Optical bench with optical path.

laser path length. The output signals from channels 1 and 2 represent horizontal and vertical displacements, respectively, of the laser-beam spot on the OPS. The input signals to channels 1 and 2 represent commands that drive FSM 1 about its vertical and horizontal axes, respectively. Input-output data from open-loop experiments showed negligible coupling between the two channels of  $P$ , so henceforth, all discussion assumes that  $P$  has two uncoupled channels, labeled as  $P_1$  and  $P_2$ , respectively. An estimate  $\hat{P}$  of  $P$  was identified as in [2] and [3]. The corresponding Bode plots are shown in Fig. 3.

For purposes of analysis, a classical LTI two-input/two-output controller  $K$ , to be connected to  $P$  according to Fig. 4, is designed as in [3]. The output disturbance  $d$  represents the combined effects of all disturbances acting on the system. The two-channel sensitivity function, mapping  $d$  to  $z$ , for the closed-loop LTI system is

$$S = (I + PK)^{-1} \quad (1)$$

with

$$P = \begin{bmatrix} P_1 & 0 \\ 0 & P_2 \end{bmatrix}, \quad K = \begin{bmatrix} K_1 & 0 \\ 0 & K_2 \end{bmatrix}. \quad (2)$$

An estimate of  $S$ ,  $\hat{S} = (I + \hat{P}K)^{-1}$ , is shown in Fig. 3. This transfer function is important because it establishes fundamental limits on the performance achievable with the observer-based controller to be presented in Section VI.

The controller  $K$ , directly connected to  $P$  as in Fig. 4, is not used in the experiments studied in this paper. However, both systems  $\hat{P}$  and  $K$  are used in the design of the proposed observer-based controller, which uses only light intensity for feedback. The mapping from the two-channel digital control command, marked by ⑥ in Fig. 1, to the sampled single photodiode sensor output, marked by ⑧ in Fig. 1, is a two-input/one-output nonlinear dynamical system. This nonlinear system can be thought of as an LTI plant  $P$  connected in series to a static function that maps the coordinates measured using the OPS to the output from a single photodiode sensor, in a Wiener-Hammerstein configuration, as depicted in Fig. 5. There,  $\psi(z)$  is the static map,  $u$  is the input command to FSM 1,  $y$  is the output from the LTI open-loop plant  $P$ , the signal  $d$  is an output disturbance modeling the total effect of the disturbances generated by FSM 2 and possibly the shaker, the signal  $z$  is the 2-D laser-beam spot position on the OPS,  $v$  is the sensor noise, and  $\phi$  is the photodiode sensor output, in volts.

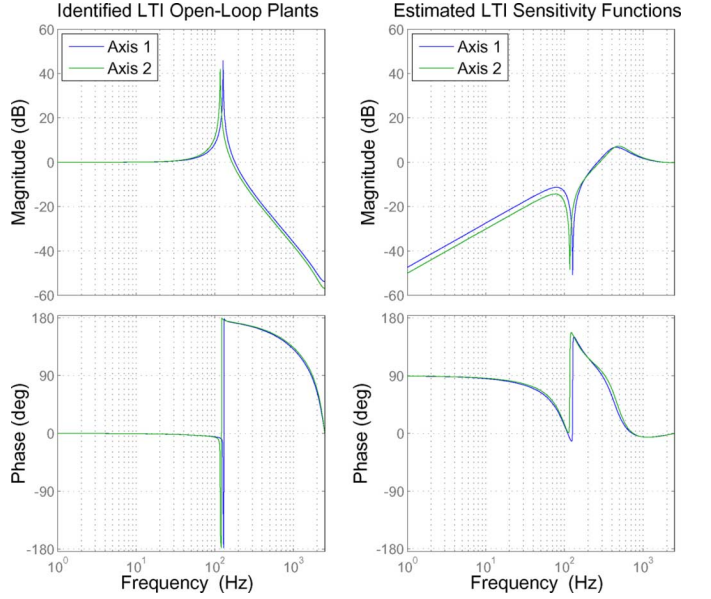


Fig. 3. *Left Plot:* Bode plots of estimated LTI open-loop plants  $\hat{P}_1$  and  $\hat{P}_2$ . *Right Plot:* Bode plots of estimated LTI output sensitivity functions  $\hat{S}_1 = (1 + \hat{P}_1 K_1)^{-1}$  and  $\hat{S}_2 = (1 + \hat{P}_2 K_2)^{-1}$ , where  $\hat{S} = \begin{bmatrix} \hat{S}_1 & 0 \\ 0 & \hat{S}_2 \end{bmatrix}$ .

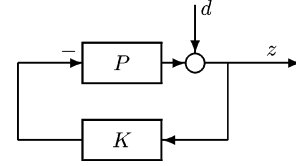


Fig. 4. Configuration used in the design of the two-input/two-output LTI controller  $K$ .  $P$ : LTI two-input/two-output open-loop plant;  $d$ : output disturbance;  $z$ : 2-D laser beam spot position on the OPS.

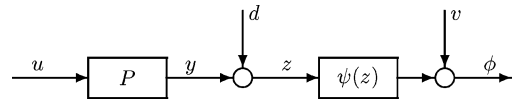


Fig. 5. Idealization of the two-input/one-output open-loop nonlinear system mapping the FSM 1 input commands to the photodiode sensor output.  $P$ : LTI open-loop plant;  $\psi(z)$ : static map;  $u$ : input command to FSM 1;  $y$ : output from LTI open-loop plant  $P$ ;  $d$ : output disturbance;  $z$ : 2-D laser beam spot position on the OPS;  $v$ : sensor noise;  $\phi$ : photodiode sensor output.

Photodiodes are solid-state devices that convert light into voltage, and therefore, the output from the photodiode sensor at position ⑦ is measured in volts. In the operation region, the photodiode voltage output is approximately linearly related to light intensity units, with a negative slope. Since this relation is approximately linear, in this work we ignore the unit transformation, and therefore, the control implementation and the data analysis are conducted using units of voltage. It is important to remark that the reason why photodiodes can be used to measure light-intensity is that there exists a static function that relates both variables in an almost linear manner [11]. We will show in Section VII that a nonlinear quadratic convex mapping  $\psi$  can be identified using the least-squares method (see Section VII and Fig. 8 therein). The fact that  $\psi$  can be modeled as a convex polynomial function depending on two variables is instrumental in determining the open-loop

observability of the optical system, and also in designing an observer for it. These two issues are addressed in the next two sections.

The decision of using a photodiode as a sensor is a response to several intellectual questions. We think that this work has immediate application to optical communications and should have future application to laser surgery. In such applications, sensors are often unavailable for measuring the position of a laser beam on a remote target or receiver, and only an optical intensity or temperature measurement at a fixed location is available for feedback control to regulate the position of the laser. Also, in cases where there exist size and weight constraints, the advantage of using a photodiode instead of a biaxial position sensor is clear. Typically, a biaxial position sensor is a box with dimensions  $10 \text{ cm} \times 10 \text{ cm} \times 4 \text{ cm}$ , weighting 300 to 400 g. On the other hand, photodiodes like the one used here have cylindrical shapes with radii ranging from 2 to 4 mm, and masses ranging from 100 to 200 mg, approximately. Notice that no improvement in performance should be expected from replacing a biaxial position sensor by a photodiode.

### III. NONLINEAR SYSTEM DYNAMICS AND OBSERVABILITY

#### A. Polynomials, Ideals, Varieties, and Observability

This paper is fundamentally experimental. However, before discussing the experimental results in Sections V–VII, we must address the issue of observability of the nonlinear system dynamics. Often in this paper, in order to distinguish from the system under control, as described in Section VI, we indistinctly refer to the original nonlinear system dynamics as the nonlinear open-loop system.

In the literature on nonlinear systems there exist several notions of observability, which are not necessarily equivalent and from which no methods for designing observers emerge naturally [8]. This is in clear contrast with the linear case, where several notions of observability are equivalent and where there exist well-known methods for designing observers. Furthermore, in the linear case there have been found connections between the observability of the open-loop system and the stability of the closed-loop system under linear quadratic regulation [12], [13], which has not been established for the general nonlinear case [7], [8].

In this section, without loss of generality and in order to simplify the algebraic manipulations, we consider the nonlinear system in Fig. 5 with  $d(t) = 0$ ,  $\forall t$ . The resulting configuration is referred henceforth as the nonlinear open-loop system, or indistinctly as nonlinear dynamics. In this case, the idea is that the system can be excited by input but not by output disturbances. We will show in Section VI that, under certain assumptions, the output signal disturbance  $d$  can be modeled as an LTI system, called disturbance model, excited by white noise. That approach leads to the formulation of an augmented Wiener-Hammerstein model capable of modeling the whole optical system in open-loop. Therefore, the analysis presented in this section can be easily extended to the augmented open-loop case.

In the optical systems considered here, modeled as Wiener-Hammerstein configurations, the static convex map is a polynomial depending on two position variables, and therefore, it can be classified as a polynomial system [8], [14], with the form

$$x(t+1) = A_P x(t) + B_P u(t) \quad (3)$$

$$y(t) = \begin{bmatrix} y_1(t) \\ y_2(t) \end{bmatrix} = C_P x(t) \quad (4)$$

$$\begin{aligned} \phi(t) &= \psi(y_1(t), y_2(t)) + v(t) = p_1 y_1^2(t) + p_2 y_2^2(t) \\ &\quad + p_{12} y_1(t) y_2(t) + q_1 y_1(t) + q_2 y_2(t) + r + v(t) \end{aligned} \quad (5)$$

in which  $x(t) \in \mathbb{R}^{n_x}$  is the system state of the LTI plant  $P$ ,  $u(t) \in \mathbb{R}^2$  is the input to the LTI system  $P$  and to the optical system as a whole,  $y(t) \in \mathbb{R}^2$  is the output from the LTI system  $P$  and the input to the nonlinear static mapping  $\psi(y_1, y_2)$  with parameters  $p_1, p_2, p_{12}, q_1, q_2, r$ , and  $v(t) \in \mathbb{R}$  is sensor noise. The corresponding state-space matrices of  $P$  are formed as

$$\begin{aligned} A_P &= \begin{bmatrix} A_{P_1} & 0 \\ 0 & A_{P_2} \end{bmatrix} \\ B_P &= \begin{bmatrix} B_{P_1} & 0 \\ 0 & B_{P_2} \end{bmatrix} \\ C_P &= \begin{bmatrix} C_{P_1} & 0 \\ 0 & C_{P_2} \end{bmatrix} \end{aligned}$$

where  $\{A_{P_1}, B_{P_1}, C_{P_1}\}$  and  $\{A_{P_2}, B_{P_2}, C_{P_2}\}$  are the sets of matrices of the state-space representations of the open-loop plants  $P_1$  and  $P_2$ , respectively. Also, we denote the sequence of inputs from 0 to  $t-1$  as  $U_t = \{u(0), u(1), \dots, u(t-1)\}$ . For this system we consider the following definition of observability.

*Definition 1 (Observability):* The system defined by (3)–(5) is observable if for each pair of initial states  $\xi \neq \eta$ , there exists a number  $N \in \mathbb{N}$  and an input sequence  $U_N$  which yields  $\phi(N, \xi, U_N) \neq \phi(N, \eta, U_N)$ .

Notice that  $U_0$  is not defined and that Definition 1 assumes  $N > 0$ . This is because for the system given by (3)–(5), an observability condition like the one in Definition 1 could never be satisfied at time 0. This follows from the fact that  $\phi(t)$  is a scalar depending on a  $2 \times 1$  vector.

As mentioned before, there are several definitions of observability when addressing nonlinear systems. The definition given above is taken from [8] in which it is referred to as multiple experiment observability. In [7], the notion of observability in Definition 1 is referred to as finite observability. There, a system is defined as observable, in the standard multiple-experiment sense, when any two initial states can be distinguished by some input/output experiment. In general, the difference between both definitions is subtle but important. Fortunately, also in [7], it is shown that for polynomial systems, both notions are equivalent. Furthermore, there, it is shown that observability, in the standard multiple-experiment sense, implies final-state determinability, which is understood as the existence of an input sequence which permits the determination of the system state resulting after this input is applied to the system.

The notion of observability in Definition 1 is deterministic and, as mentioned before, no method emerges naturally from it

for designing observers. However, as argued in [7], the cases in which it is known how to design observers in a stochastic setting, for deterministic systems, strongly suggest that estimation is feasible only when the systems involved satisfy fundamental and general notions of observability. This is relevant because, at an intuitive level, a connection, between standard multiple-experiment observability and the heuristic method employed in the experiments described in this paper, can be argued. The development and analysis of rigorous methods, for designing observers for the class of system considered here, is a matter of further research.

With the previous ideas in mind, we describe a method for evaluating the observability of systems with the form given by (3)–(5), according to Definition 1. In order to achieve this objective, first we define some fundamental concepts on *polynomials, ideals and varieties* that will be used later in this article. For a complete and detailed treatment of these topics we refer the reader to [15].

*Definition 2 (Monomial):* A monomial in  $\xi_1, \dots, \xi_n$  is a product of the form

$$\xi_1^{b_1} \cdot \xi_2^{b_2} \dots \xi_n^{b_n} \quad (6)$$

where all of the exponents  $b_1, \dots, b_n$  are nonnegative integers.

The total degree of this monomial is the sum  $b_1 + \dots + b_n$ . Usually, the notation is simplified by letting  $b = (b_1, \dots, b_n)$  be an  $n$ -tuple of nonnegative integers. Then, we write

$$\xi^b = \xi_1^{b_1} \cdot \xi_2^{b_2} \dots \xi_n^{b_n}. \quad (7)$$

This definition seems futile. However, henceforth, Definition 2 is used to simplify the notation.

*Definition 3 (Polynomial):* A polynomial  $f$  in  $\xi_1, \dots, \xi_n$  with coefficients in a field  $\mathbb{K}$  is a finite linear combination, with coefficients in  $\mathbb{K}$ , of monomials. This can be written as

$$f = \sum_b \alpha_b \xi^b, \quad \alpha_b \in \mathbb{K} \quad (8)$$

where the sum is over a finite number of  $n$ -tuples  $b = (b_1, \dots, b_n)$ . The set of all polynomials in  $\xi_1, \dots, \xi_n$  with coefficients in  $\mathbb{K}$  is denoted  $\mathbb{K}[\xi_1, \dots, \xi_n]$ .

It should be mentioned that  $\mathbb{K}[\xi_1, \dots, \xi_n]$  is a *commutative ring*, because under addition and multiplication, it satisfies all the field axioms except for the existence of multiplicative inverses. For that reason, structures with the form of  $\mathbb{K}[\xi_1, \dots, \xi_n]$  are referred to as *polynomial rings* [15].

*Definition 4 (Variety):* Let  $\mathbb{K}$  be a field, and let  $f_1, \dots, f_s$  be polynomials in  $\mathbb{K}[\xi_1, \dots, \xi_n]$ . Then it is defined

$$V(f_1, \dots, f_s) = \{(a_1, \dots, a_n) \in \mathbb{K}^n : f_i(a_1, \dots, a_n) = 0, \forall 1 \leq i \leq s\}. \quad (9)$$

The region  $V(f_1, \dots, f_s)$  is called the *affine variety* defined by  $f_1, \dots, f_s$ .

*Definition 5 (Ideal):* A subset  $I \subset \mathbb{K}[\xi_1, \dots, \xi_n]$  is an *ideal* if it satisfies the following:

- 1)  $0 \in I$ ;
- 2) if  $f, g \in I$ , then  $f + g \in I$ ;
- 3) if  $f \in I$  and  $h \in \mathbb{K}[\xi_1, \dots, \xi_n]$ , then  $hf \in I$ .

*Definition 6:* Let  $f_1, \dots, f_s$  be polynomials in  $\mathbb{K}[\xi_1, \dots, \xi_n]$ . Then it is defined

$$\langle f_1, \dots, f_s \rangle = \left\{ \sum_{i=1}^s h_i f_i : h_1, \dots, h_s \in \mathbb{K}[\xi_1, \dots, \xi_n] \right\}. \quad (10)$$

An important thing to notice and know is that  $\langle f_1, \dots, f_s \rangle$  is an ideal. This is written below, as a lemma taken from [15].

*Lemma 1:* If  $f_1, \dots, f_s \in \mathbb{K}[\xi_1, \dots, \xi_n]$ , then  $\langle f_1, \dots, f_s \rangle$  is an ideal of  $\mathbb{K}[\xi_1, \dots, \xi_n]$ . Commonly,  $\langle f_1, \dots, f_s \rangle$  is called the *ideal generated by  $f_1, \dots, f_s$* .

*Proof:* See [15, Ch. 1].

Finally in this subsection, we state the most important conceptual tool used for determining the observability of the open-loop nonlinear system.

*Lemma 2:* If  $f_1, \dots, f_s$  and  $g_1, \dots, g_t$  are bases of the same ideal in  $\mathbb{K}[\xi_1, \dots, \xi_n]$ , i.e.,  $\langle f_1, \dots, f_s \rangle = \langle g_1, \dots, g_t \rangle$ , then  $V(f_1, \dots, f_s) = V(g_1, \dots, g_t)$ .

*Proof:* See [15, Ch. 1].

## B. Gröbner Bases

An important concept used in the rest of this article is the one referred as Gröbner bases. In difficult cases, the Gröbner bases method allows us to determine if a given polynomial belongs to a given ideal, and also to determine if two ideals, generated by two different sets of polynomials, are equal or not. In general, the Gröbner bases method is used to transform a polynomial set  $F \in \mathbb{K}[\xi_1, \dots, \xi_n]$  into a reduced polynomial set  $G \in \mathbb{K}[\xi_1, \dots, \xi_n]$ , such that both sets are equivalent in the sense that both generate the same ideal, i.e.,  $\langle F \rangle = \langle G \rangle$ . The new set  $G$  is called a Gröbner basis. For a fixed polynomial ordering (in this report we use a lexicographic ordering [15]), the Gröbner basis of a polynomial set is unique. For further details and for the algorithm see [15] and [16].

## C. Determining the Observability of the Open-Loop System

In this subsection, using an adapted version of the method in [8], we exemplify a way to determine if the nonlinear open-loop system in (3)–(5) is observable according to Definition 1. The method is based on Lemma 2 and on the concept of Gröbner bases described in the previous subsections. Obviously, in this article, the signal of interest is the output  $\phi(t)$  in (5), which depends indirectly on  $t$ , and directly on the initial condition of the system and on the sequence inputted to it. Thus,  $\phi(0, \xi)$  refers to the output of the system at time 0 with initial condition  $\xi$ . Clearly,  $\phi(t, \xi, U_t)$  refers to the output of the system at time  $t$ , with initial condition  $\xi$  and sequence of inputs  $U_t$ .

According to Definition 1, if it is possible to find two initial states  $\xi$  and  $\eta$  such that  $\xi \neq \eta$  for which  $\phi(0, \xi) = \phi(0, \eta)$  and  $\phi(t, \xi, U_t) = \phi(t, \eta, U_t)$  for  $t > 0$ , for each possible sequence  $U_t$ , then the system in (3)–(5) is not observable. With this in mind, we construct a sequence of ideals  $J_t \subset \mathbb{R}[\xi_1, \xi_2, \dots, \xi_{n_x}, \eta_1, \eta_2, \dots, \eta_{n_x}]$ ,  $t = 0, 1, \dots$ , generated by the outputs of the system from 0 to  $t$ , assuming that  $\phi(0, \xi) = \phi(0, \eta)$  and  $\phi(t, \xi, U_t) = \phi(t, \eta, U_t)$  for  $t > 0$ . Then, if the logical conclusion is that the previous condition is satisfied if and only if there exists a positive integer  $N$  such that  $\xi = \eta$  for at least one possible sequence  $U_N$ , then the system

is observable. This analysis can be done using the concept of variety in Definition 4, as it is done in [8] for a different class of polynomial nonlinear systems.

Notice that by construction  $J_0 \subseteq J_1 \subseteq J_2 \subseteq J_3 \dots$ . Also, from [15], [17] and [8], we know that for the sequence of ideals  $J_t$ ,  $t \geq 0$ , for the class of polynomial systems considered here, there exists a termination integer  $N_T$  such that  $J_{N_T} = J_{N_T+1}$ . This equality can be determined by using the concept of Gröbner bases described in the previous subsection. We denote the Gröbner basis associated to a generic ideal  $J_t$  by  $\mathcal{B}_G[J_t]$ . Also, notice that by Lemma 2, the variety  $V(\mathcal{B}_G[J_t])$  is identical to the variety of the original set of polynomials that generates  $J_t$ .

From the previous paragraph a natural method for determining observability emerges because if

$$V(\mathcal{B}_G[J_{N_T}]) \cap \{(\xi, \eta) : \xi \neq \eta\} = \emptyset \quad (11)$$

then, the system is observable according to Definition 1. This follows from noticing that (11) is equivalent to saying that  $\xi = \eta$  if and only if  $\phi(0, \eta) = \phi(0, \xi)$  and  $\phi(t, \eta, U_t) = \phi(t, \xi, U_t)$  for  $0 < t \leq N_T$ , for at least one possible sequence  $U_{N_T}$ . In fact, if (11) is satisfied,  $\xi = \eta$  implies that  $\phi(0, \eta) = \phi(0, \xi)$  and  $\phi(t, \eta, U_t) = \phi(t, \xi, U_t)$  for  $0 < t \leq N_T$ , for each possible sequence  $U_{N_T}$ . Also,  $\phi(0, \eta) = \phi(0, \xi)$ ,  $\phi(t, \eta, U_t) = \phi(t, \xi, U_t)$  for  $0 < t \leq N_T$  implies that  $\xi = \eta$ , for *almost* any arbitrarily chosen sequence  $U_{N_T}$ . In [8] it is suggested that in order to determine if an expression with the form of (11) is true or not, a logical decision problem can be formulated and then solved using QEPCAD<sup>1</sup> [18]. Being QEPCAD an excellent toolbox, it has the inconvenience that it only accepts integer parameters. Fortunately, in the cases relevant for this work, there exists a way around this issue. Notice, that if  $\mathcal{B}_G[J_{N_T}] = \{\xi_1 - \eta_1, \xi_2 - \eta_2, \dots, \xi_{n_x} - \eta_{n_x}\}$ , then (11) is true and consequently the system is observable. To show how the method can be applied to our case, here, three examples are presented.

1) *Example 1:* First, we analyze a simple and easy case, that nonetheless, allows us to extract some important conclusions. Consider the system

$$\begin{aligned} \begin{bmatrix} x_1(t+1) \\ x_2(t+1) \end{bmatrix} &= \begin{bmatrix} 0.5x_1(t) + u_1(t) \\ 0.5x_2(t) + u_2(t) \end{bmatrix} \\ \begin{bmatrix} y_1(t) \\ y_2(t) \end{bmatrix} &= \begin{bmatrix} x_1(t) \\ x_2(t) \end{bmatrix} \\ \phi(t) &= y_1^2(t) + y_2^2(t). \end{aligned}$$

Then, considering an arbitrary sequence of inputs  $U_t = \{u(0), u(1), \dots, u(t-1)\}$ , we have that for  $t = 0$

$$\phi(0) = x_1^2(0) + x_2^2(0)$$

which implies that

$$\phi(0, \eta) - \phi(0, \xi) = \eta_1^2 - \xi_1^2 + \eta_2^2 - \xi_2^2$$

and consequently, that the ideal  $J_0 = \langle \mathcal{P}_0 \rangle$  is generated by

$$\mathcal{P}_0 = \{\eta_1^2 - \xi_1^2 + \eta_2^2 - \xi_2^2\}.$$

It is immediately clear that  $\mathcal{B}_G[J_0] = \{\eta_1^2 - \xi_1^2 + \eta_2^2 - \xi_2^2\}$ . For  $t = 1$ , we have that

$$\begin{aligned} \phi(1) &= 0.25x_1^2(0) + x_1(0)u_1(0) + u_1^2(0) + 0.25x_2^2(0) \\ &\quad + x_2(0)u_2(0) + u_2^2(0) \end{aligned}$$

which implies that

$$\begin{aligned} \phi(1, \eta, U_1) - \phi(1, \xi, U_1) &= 0.25\eta_1^2 - 0.25\xi_1^2 + 0.25\eta_2^2 - 0.25\xi_2^2 \\ &\quad + (\eta_1 - \xi_1)u_1(0) + (\eta_2 - \xi_2)u_2(0) \end{aligned}$$

and consequently, that the ideal  $J_1 = \langle \mathcal{P}_1 \rangle$  is generated by

$$\begin{aligned} \mathcal{P}_1 &= \{\eta_1^2 - \xi_1^2 + \eta_2^2 - \xi_2^2; 0.25\eta_1^2 - 0.25\xi_1^2 + 0.25\eta_2^2 \\ &\quad - 0.25\xi_2^2; \eta_1 - \xi_1; \eta_2 - \xi_2\}. \end{aligned}$$

Using the function *groebner* in [19], it can be determined that the Gröbner basis associated to  $J_1$  is

$$\mathcal{B}_G[\langle \mathcal{P}_1 \rangle] = \{\eta_1 - \xi_1; \eta_2 - \xi_2\}.$$

As explained before, this implies that  $N_T = 1$ , and therefore, that the system considered in this example is observable according to Definition 1.

Now, we look at the issue of empirically assessing how difficult it is to find an input sequence  $U_1$  capable of distinguishing between two different initial states. Consider the case  $\eta_1 = 1$ ,  $\xi_1 = -1$ ,  $\eta_2 = -1$ ,  $\xi_2 = 1$ . If we were to choose  $u_1(0) = 0$ ,  $u_2(0) = 0$ , these two initial states cannot be distinguished. However, almost any other arbitrarily chosen input sequence is capable of distinguishing these two different initial states. To support this statement, 500 experiments were conducted in MATLAB, in which  $U_1$  was chosen at random using the function *randn*. In all those 500 computer experiments, the resulting  $U_1$  was capable of distinguishing between the two different states. This strongly suggests that finding distinguishing inputs is not a difficult task in this case. Also, that if an observer was to be implemented, a biased input signal might be required, in order to avoid zero-crossings as much as possible. Furthermore, it is interesting to note that the states in this particular case cannot be distinguished by signals with the form  $u_1(0) = u_2(0) \in \mathbb{R}$ . The next example is used to suggest that, for some particular states, it appears to be a connection between the minimizing point  $y^* = \{y_1^*, y_2^*\}$  of the surface  $\psi(y_1, y_2)$  and the required bias to be chosen for the input distinguishing signal. This is a matter of further research, the topic will be addressed in a future publication.

2) *Example 2:* Consider the same system than in Example 1, but with

$$\phi(t) = y_1^2(t) + y_2^2(t) + 3y_1(t) + 2y_2(t).$$

<sup>1</sup>Quantifier Elimination by Partial Cylindrical Algebraic Decomposition.

Then, skipping some steps already shown in Example 1, it follows that for  $t = 0$

$$\phi(0, \eta) - \phi(0, \xi) = \eta_1^2 - \xi_1^2 + \eta_2^2 - \xi_2^2 + 3\eta_1 - 3\xi_1 + 2\eta_2 - 2\xi_2$$

and that

$$\mathcal{B}_G [J_0] = \{ \eta_1^2 - \xi_1^2 + \eta_2^2 - \xi_2^2 + 3\eta_1 - 3\xi_1 + 2\eta_2 - 2\xi_2 \}.$$

For  $t = 1$ , we have that

$$\begin{aligned} \phi(1, \eta, U_1) - \phi(1, \xi, U_1) &= 0.25\eta_1^2 - 0.25\xi_1^2 + 0.25\eta_2^2 - 0.25\xi_2^2 \\ &\quad + 1.5\eta_1 - 1.5\xi_1 + \eta_2 - \xi_2 \\ &\quad + (\eta_1 - \xi_1)u_1(0) + (\eta_2 - \xi_2)u_2(0) \end{aligned}$$

and consequently, that the ideal  $J_1 = \langle \mathcal{P}_1 \rangle$  is generated by

$$\begin{aligned} \mathcal{P}_1 &= \{ \eta_1^2 - \xi_1^2 + \eta_2^2 - \xi_2^2 + 3\eta_1 - 3\xi_1 + 2\eta_2 - 2\xi_2; \\ &\quad 0.25\eta_1^2 - 0.25\xi_1^2 + 0.25\eta_2^2 - 0.25\xi_2^2 + 1.5\eta_1 - 1.5\xi_1 \\ &\quad + \eta_2 - \xi_2; \eta_1 - \xi_1; \eta_2 - \xi_2 \}. \end{aligned}$$

Using the function *groebner* in [19], it can be determined that the Gröbner basis associated to  $J_1$  is

$$\mathcal{B}_G [\langle \mathcal{P}_1 \rangle] = \{ \eta_1 - \xi_1; \eta_2 - \xi_2 \}.$$

Again, this implies that  $N_T = 1$  and that the system is observable according to Definition 1.

In this case, for  $\eta_1 = 1$ ,  $\xi_1 = -1$ ,  $\eta_2 = -1.5$ ,  $\xi_2 = 1.5$ , if we were to choose  $u_1(0) = -3/2$  and  $u_2(0) = -1$ , these two states cannot be distinguished. Furthermore, they cannot be distinguished by signals with the form  $u_1(0) = (3/2)u_2(0) \in \mathbb{R}$ , which is the same that to say that these particular states are indistinguishable by signals with the form  $u(0) = y^* \lambda$ , where  $\lambda \in \mathbb{R}$  and  $y^*$  is the minimizing point of the surface  $\psi(y_1, y_2)$ . At this point, it is not obvious if this is a random coincidence or the indication of a pattern. However, as in Example 1, this is an interesting phenomenon because almost any vector generated at random, as tested using MATLAB, is a distinguishing signal  $U_1$ . As mentioned before, this is an issue to be addressed by further research in the future.

3) *Example 3:* This case is interesting because the models used in this analysis are the ones obtained by system identification, according to the methods described in Section II. As explained in [3], the LTI identified model  $\hat{P}$ , depending on the dynamics of the microelectromechanical mirror FSM 1 and on the OPS, remains essentially the same regardless of the optical configuration of the experimental setup in Figs. 1 and 2. However, the identified mapping  $\psi$  depends greatly on the power of the laser-beam, the characteristics of the beam splitter, the incident angle of the laser-beam on the photodiode, and on the electronic circuit used to feed the photodiode. Clearly, the open-loop observability of the system depends not only on the parameters of the identified plant  $\hat{P}$  but also on the parameters of  $\psi$ . This suggests that in some optical configurations, even slightly different to the one employed in the experiments presented in this paper, the resulting nonlinear system might not be observable, according to Definition 1, though, this phenomenon

has not been observed by these authors yet. Consider the system formed by (3)–(5) with the identified matrices

$$\begin{aligned} A_P &= \begin{bmatrix} 0.9869 & -0.1592 & 0 & 0 \\ 0.1592 & 0.9868 & 0 & 0 \\ 0 & 0 & 0.9887 & -0.1462 \\ 0 & 0 & 0.1462 & 0.9886 \end{bmatrix} \\ B_P &= \begin{bmatrix} 1.6131 & 0 \\ -1.5277 & 0 \\ 0 & 1.9522 \\ 0 & -1.8469 \end{bmatrix} \\ C_P &= \begin{bmatrix} 0.0522 & 0.0495 & 0 & 0 \\ 0 & 0 & 0.0396 & 0.0375 \end{bmatrix} \end{aligned}$$

and the identified parameters  $p_1 = 0.0201$ ,  $p_2 = 0.0342$ ,  $p_{12} = -0.0067$ ,  $q_1 = -0.0261$ ,  $q_2 = 0.0148$ , and  $r = 0.4679$ . In order to simplify the notation, we define  $\alpha(t) = C_{P_1} A_{P_1}^t$ ,  $\gamma(t) = C_{P_2} A_{P_2}^t$ ,  $\beta(t) = C_{P_1} A_{P_1}^t B_{P_1}$ , and  $\delta(t) = C_{P_2} A_{P_2}^t B_{P_2}$  for  $t \geq 0$ . Then, it is immediately obvious that

$$\begin{aligned} \phi(t) &= p_1 \left[ \alpha(t) \begin{bmatrix} x_1(0) \\ x_2(0) \end{bmatrix} + \sum_{i=0}^{t-1} \beta(t-i-1)u_1(i) \right]^2 \\ &\quad + p_2 \left[ \gamma(t) \begin{bmatrix} x_3(0) \\ x_4(0) \end{bmatrix} + \sum_{i=0}^{t-1} \delta(t-i-1)u_2(i) \right]^2 \\ &\quad + p_{12} \left[ \alpha(t) \begin{bmatrix} x_1(0) \\ x_2(0) \end{bmatrix} + \sum_{i=0}^{t-1} \beta(t-i-1)u_1(i) \right] \\ &\quad \cdot \left[ \gamma(t) \begin{bmatrix} x_3(0) \\ x_4(0) \end{bmatrix} + \sum_{i=0}^{t-1} \delta(t-i-1)u_2(i) \right] \\ &\quad + q_1 \left[ \alpha(t) \begin{bmatrix} x_1(0) \\ x_2(0) \end{bmatrix} + \sum_{i=0}^{t-1} \beta(t-i-1)u_1(i) \right] \\ &\quad + q_2 \left[ \gamma(t) \begin{bmatrix} x_3(0) \\ x_4(0) \end{bmatrix} + \sum_{i=0}^{t-1} \delta(t-i-1)u_2(i) \right] + r \end{aligned}$$

and consequently, the sequence of ideals  $J_t$ , assuming  $\phi(t, x(0) = \eta) = \phi(t, x(0) = \xi)$ ,  $t > 0$  is formed as follows.

For  $t = 0$ , the ideal  $J_0 = \langle \mathcal{P}_0 \rangle$  is generated by the set  $\mathcal{P}_0$  that contains only the polynomial

$$\begin{aligned} \mathcal{P}_0 &= \{ p_1 \alpha_1^2(0) (\eta_1^2 - \xi_1^2) + p_1 \alpha_2^2(0) (\eta_2^2 - \xi_2^2) \\ &\quad + 2p_1 \alpha_1(0) \alpha_2(0) (\eta_1 \eta_2 - \xi_1 \xi_2) + p_2 \gamma_1^2(0) (\eta_3^2 - \xi_3^2) \\ &\quad + p_2 \gamma_2^2(0) (\eta_4^2 - \xi_4^2) + 2p_2 \gamma_1(0) \gamma_2(0) (\eta_3 \eta_4 - \xi_3 \xi_4) \\ &\quad + p_{12} \alpha_1(0) \gamma_1(0) (\eta_1 \eta_3 - \xi_1 \xi_3) \\ &\quad + p_{12} \alpha_1(0) \gamma_2(0) (\eta_1 \eta_4 - \xi_1 \xi_4) \\ &\quad + p_{12} \alpha_2(0) \gamma_1(0) (\eta_2 \eta_3 - \xi_2 \xi_3) \\ &\quad + p_{12} \alpha_2(0) \gamma_2(0) (\eta_2 \eta_4 - \xi_2 \xi_4) \\ &\quad + q_1 \alpha_1(0) (\eta_1 - \xi_1) + q_1 \alpha_2(0) (\eta_2 - \xi_2) \\ &\quad + q_2 \gamma_1(0) (\eta_3 - \xi_3) + q_2 \gamma_2(0) (\eta_4 - \xi_4) \}. \end{aligned}$$

In this case, using the function *groebner* in [19], it can be determined that the Gröbner basis  $\mathcal{B}_G [J_0]$  is one long polynomial.

For  $t = 1$ , the ideal  $J_1$  is generated by the set

$$\mathcal{P}_1 = \{ \mathcal{P}_0; p_1 \alpha_1^2(1) (\eta_1^2 - \xi_1^2) \}$$

$$\begin{aligned}
& + 2p_1\alpha_1(1)\alpha_2(1)(\eta_1\eta_2 - \xi_1\xi_2) \\
& + p_1\alpha_2^2(1)(\eta_2^2 - \xi_2^2) + p_2\gamma_1^2(1)(\eta_3^2 - \xi_3^2) \\
& + 2p_2\gamma_1(1)\gamma_2(1)(\eta_3\eta_4 - \xi_3\xi_4) + p_2\gamma_2^2(1)(\eta_4^2 - \xi_4^2) \\
& + p_{12}\alpha_1(1)\gamma_1(1)(\eta_1\eta_3 - \xi_1\xi_3) \\
& + p_{12}\alpha_1(1)\gamma_2(1)(\eta_1\eta_4 - \xi_1\xi_4) \\
& + p_{12}\alpha_2(1)\gamma_1(1)(\eta_2\eta_3 - \xi_2\xi_3) \\
& + p_{12}\alpha_2(1)\gamma_2(1)(\eta_2\eta_4 - \xi_2\xi_4) \\
& + q_1\alpha_1(1)(\eta_1 - \xi_1) + q_1\alpha_2(1)(\eta_2 - \xi_2) \\
& + q_2\gamma_1(1)(\eta_3 - \xi_3) + q_2\gamma_2(1)(\eta_4 - \xi_4); \\
& 2p_1\beta(0)\alpha_1(1)(\eta_1 - \xi_1) + 2p_1\beta(0)\alpha_2(1)(\eta_2 - \xi_2) \\
& + p_{12}\beta(0)\gamma_1(1)(\eta_3 - \xi_3) + p_{12}\beta(0)\gamma_2(1)(\eta_4 - \xi_4); \\
& 2p_2\delta(0)\gamma_1(1)(\eta_3 - \xi_3) + 2p_2\delta(0)\gamma_2(1)(\eta_4 - \xi_4) \\
& + p_{12}\delta(0)\alpha_1(1)(\eta_1 - \xi_1) + p_{12}\delta(0)\alpha_2(1)(\eta_2 - \xi_2) \}.
\end{aligned}$$

Using the function *groebner* in [19], it can be determined that the Gröbner basis  $\mathcal{B}_G [J_1]$  is composed of long polynomials and that  $J_1 \neq J_0$ .

For  $t = 2$ , the ideal  $J_2$  is generated by the set

$$\begin{aligned}
\mathcal{P}_2 = \{ & \mathcal{P}_1; p_1\alpha_1^2(2)(\eta_1^2 - \xi_1^2) \\
& + 2p_1\alpha_1(2)\alpha_2(2)(\eta_1\eta_2 - \xi_1\xi_2) \\
& + p_1\alpha_2^2(2)(\eta_2^2 - \xi_2^2) + p_2\gamma_1^2(2)(\eta_3^2 - \xi_3^2) \\
& + 2p_2\gamma_1(2)\gamma_2(2)(\eta_3\eta_4 - \xi_3\xi_4) + p_2\gamma_2^2(2)(\eta_4^2 - \xi_4^2) \\
& + p_{12}\alpha_1(2)\gamma_1(2)(\eta_1\eta_3 - \xi_1\xi_3) \\
& + p_{12}\alpha_1(2)\gamma_2(2)(\eta_1\eta_4 - \xi_1\xi_4) \\
& + p_{12}\alpha_2(2)\gamma_1(2)(\eta_2\eta_3 - \xi_2\xi_3) \\
& + p_{12}\alpha_2(2)\gamma_2(2)(\eta_2\eta_4 - \xi_2\xi_4) \\
& + q_1\alpha_1(2)(\eta_1 - \xi_1) + q_1\alpha_2(2)(\eta_2 - \xi_2) \\
& + q_2\gamma_1(2)(\eta_3 - \xi_3) + q_2\gamma_2(2)(\eta_4 - \xi_4); \\
& 2p_1\alpha_1(2)\beta(1)(\eta_1 - \xi_1) + 2p_1\alpha_2(2)\beta(1)(\eta_2 - \xi_2) \\
& + p_{12}\gamma_1(2)\beta(1)(\eta_3 - \xi_3) + p_{12}\gamma_2(2)\beta(1)(\eta_4 - \xi_4); \\
& 2p_1\alpha_1(2)\beta(0)(\eta_1 - \xi_1) + 2p_1\alpha_2(2)\beta(0)(\eta_2 - \xi_2) \\
& + p_{12}\gamma_1(2)\beta(0)(\eta_3 - \xi_3) + p_{12}\gamma_2(2)\beta(0)(\eta_4 - \xi_4); \\
& 2p_2\gamma_1(2)\delta(1)(\eta_3 - \xi_3) + 2p_2\gamma_2(2)\delta(1)(\eta_4 - \xi_4) \\
& + p_{12}\alpha_1(2)\delta(1)(\eta_1 - \xi_1) + p_{12}\alpha_2(2)\delta(1)(\eta_2 - \xi_2); \\
& 2p_2\gamma_1(2)\delta(0)(\eta_3 - \xi_3) + 2p_2\gamma_2(2)\delta(0)(\eta_4 - \xi_4) \\
& + p_{12}\alpha_1(2)\delta(0)(\eta_1 - \xi_1) + p_{12}\alpha_2(2)\delta(0)(\eta_2 - \xi_2) \}.
\end{aligned}$$

Using the function *groebner* in [19], it can be determined that the Gröbner basis associated to  $J_2$  is

$$\mathcal{B}_G [\langle \mathcal{P}_2 \rangle] = \{\eta_1 - \xi_1; \eta_2 - \xi_2; \eta_3 - \xi_3; \eta_4 - \xi_4\}.$$

As explained before, this implies that  $N_T = 2$ , and therefore, that the system considered in this example is observable according to Definition 1.

From this example it is possible to conclude that in general the observability of a system with the form of (3)–(5) depends on the identified matrices  $A_p$ ,  $B_p$ , and  $C_p$  of the linear part of the system and on the identified parameters  $p_1$ ,  $p_2$ ,  $p_{12}$ ,  $q_1$ , and  $q_2$  of the nonlinear static map of the system. This tells us that

there exists a general criterion for determining the observability of the system, which will be addressed in a future publication.

To the best of our knowledge, this is the first time that a Gröbner bases-based method is used to determine the observability of systems with the form given by (3)–(5), using the MATLAB function *groebner* in [19]. The accuracy of the results produced by this function depends on several tuning parameters. Therefore, in order to facilitate the verification and reproducibility of the results presented in the previous examples, the generating polynomial sets are explicitly shown. It is important to mention that most of the tedious algebra necessary to find the generating polynomials has been omitted.

#### IV. REVIEW OF THE EXTENDED KALMAN FILTER

As mentioned before, for the class of nonlinear models describing the optical system in Section II, there is not a *known* direct natural connection between the general notion of observability in Definition 1 with the heuristic methods for designing observers for nonlinear systems. However, as mentioned in Section III based on the arguments in [7], the fact that the system considered here, described in Example 3, is observable according to Definition 1 suggests that the employment of an observer, designed in a stochastic setting, is reasonable. Here, we empirically investigate the feasibility of employing the extended Kalman filter.

In general, a nonlinear dynamic system can be written as

$$x(t+1) = f(x(t), w(t)) \quad (12)$$

$$\phi(t) = g(x(t), v(t)) \quad (13)$$

where  $f$  and  $g$  are possibly nonlinear functions, and  $w$  and  $v$  are stationary zero-mean white random processes with

$$E \begin{bmatrix} w(t) \\ v(t) \\ x(0) - \bar{x}_0 \end{bmatrix} \begin{bmatrix} w(t) \\ v(t) \\ x(0) - \bar{x}_0 \end{bmatrix}^T = \begin{bmatrix} \Sigma_w & 0 & \\ 0 & \Sigma_v & 0 \\ 0 & 0 & \Sigma_0 \end{bmatrix} \quad (14)$$

where  $\bar{x}_0 = E[x(0)]$ .

Regardless of the model, the least-mean-squares predictor of the state vector  $x(t)$ , based on the past observed outputs, and the least-mean-squares estimator of the state vector  $x(t)$ , based on the current and past observed outputs, at any particular time instant  $t$ , are given by the conditional means [9], [10], [20], i.e.,

$$\hat{x}(t|t-1) = E[x(t)|\Phi(t-1)] \quad (15)$$

$$\hat{x}(t|t) = E[x(t)|\Phi(t)] \quad (16)$$

where  $\Phi(t-1) = \{\phi(\sigma), 0 < \sigma < t-1\}$  and  $\Phi(t) = \{\phi(\sigma), 0 < \sigma < t\}$ .

Finding explicit formulas for (15) and (16) is almost always very difficult. A heuristic approach to this problem is the EKF [9], [10], which is based on linearizing the dynamics and output functions at current estimate, and on propagating an approximation of the conditional expectation and covariance. The resulting algorithm as presented in [9] is as follows.

*Algorithm 1 (EKF):* Consider the model (12)–(13) with conditions (14). An approximate estimator for the state  $x(t)$  can be recursively computed as follows.

- *Initialization:*  $\hat{x}(0| - 1) = \bar{x}_0, \Sigma_{0|-1} = \Sigma_0$ .
- *Linearize output function at  $x = \hat{x}(t|t - 1)$ :*

$$\zeta = \frac{\partial g}{\partial x}(\hat{x}(t|t - 1), 0) \quad (17)$$

$$V = \frac{\partial g}{\partial v}(\hat{x}(t|t - 1), 0) \Sigma_v \left[ \frac{\partial g}{\partial v}(\hat{x}(t|t - 1), 0) \right]^T. \quad (18)$$

- *Update measurements based on linearization:*

$$\hat{x}(t|t) = \hat{x}(t|t - 1) + \kappa_t (\phi(t) - g(\hat{x}(t|t - 1), 0)) \quad (19)$$

$$\Sigma_{t|t} = \Sigma_{t|t-1} - \kappa_t \zeta \Sigma_{t|t-1} \quad (20)$$

with

$$\kappa_t = \Sigma_{t|t-1} \zeta^T (\zeta \Sigma_{t|t-1} \zeta^T + V)^{-1}. \quad (21)$$

- *Linearize dynamics function at  $x = \hat{x}(t|t)$ :*

$$A = \frac{\partial f}{\partial x}(\hat{x}(t|t), 0) \quad (22)$$

$$W = \frac{\partial f}{\partial w}(\hat{x}(t|t), 0) \Sigma_w \left[ \frac{\partial f}{\partial w}(\hat{x}(t|t), 0) \right]^T. \quad (23)$$

- *Update time based on linearization:*

$$\hat{x}(t + 1|t) = f(\hat{x}(t|t), 0) \quad (24)$$

$$\Sigma_{t+1|t} = A \Sigma_{t|t} A^T + W. \quad (25)$$

◇

Despite being a heuristic method, during the last three decades, the EKF has received significant attention from control theorists, who have studied the convergence and stability properties of the algorithm [21]–[25]. In particular, [22] shows that the EKF is a quasi-local asymptotic observer for discrete-time nonlinear systems. There, stochastic nonlinear systems are assumed in the design of EKFs, intended to be used as observers for a deterministic nonlinear systems. The analysis presented in [22] establishes that the boundedness of the error covariances, necessary for the convergence of the estimation error, is achieved if an observability condition is satisfied on the linearization of the nonlinear system along the estimated trajectory. Additionally, in order to have convergence of the estimation error, the nonlinear system has to satisfy a series of assumptions, among them that the Euclidean norm of the initial estimation error,  $|e_x(0)| = |x(0) - \hat{x}(0| - 1)|$ , must be bounded by specific quantities, which depend on the parameters of the specific nonlinear system considered.

In practice, the theoretical conditions required for enforcing the convergence or boundedness of the EKF's estimation error, commented in the previous paragraph, are impossible or extremely difficult to verify. Additionally to this, in general, EKF-based observers do not satisfy the conditions required for guaranteeing the global asymptotic stability (GAS) of the estimation error dynamics. Furthermore, the convergence and stability analysis of closed-loop systems that rely on EKF-based observers remains an open problem. For these reasons, in this work as in most industrial and experimental applications, the employed EKF-based observers are empirically tuned and tested.

## V. IMPLEMENTATION OF THE OBSERVER IN OPEN-LOOP

In this section, we test the suitability of the EKF algorithm for estimating the state  $x$ , and the output  $y$  of the linear part of the system in open-loop. The system to consider is given by

$$\begin{aligned} x(t + 1) &= f(x(t), w_P(t), u(t)) \\ &= A_P x(t) + B_P w_P(t) + B_P u(t) \end{aligned} \quad (26)$$

with linear and nonlinear outputs  $y(t)$  and  $\phi(t)$  given by (4) and (5), respectively. The matrices  $A_P, B_P, C_P$  and the parameters for  $\psi(y_1, y_2)$  are the same as those in Example 3. As mentioned in Sections II and III,  $v(t) \in \mathbb{R}$  is sensor noise, but in this section for purposes of analysis and design it is assumed to be white stationary and zero-mean. A difference of this system with the one considered in Section III is the inclusion of the term  $B_P w_P(t)$ . Here,  $w_P(t) \in \mathbb{R}^2$  is an input disturbance to the system, which can be thought of as an unknown deterministic, or, for purposes of analysis and design, as a stochastic disturbance. In either case, the new element  $B_P w_P(t)$  would not change the observability of the system, from an abstract viewpoint, since the analysis in Example 3 would remain essentially unchanged if this new term was to be included.

As explained before, observability according to Definition 1 does not guarantee that the EKF method, which is a heuristic solution, would yield satisfactory results. In order to implement and test the method, we assume that  $w_P$  and  $v$  are stationary zero-mean white random processes, and with the initial condition  $x(0)$ , satisfy the condition in (14). Notice that since (26) depends on  $u(t)$ , its form is slightly different from the one of (12). However, this will not modify the EKF design algorithm significantly, because  $u(t)$  is known by the observer. Thus, the only thing to change is the way in which the system state estimate is time-updated, i.e., (24) is replaced by

$$\hat{x}(t + 1|t) = f(\hat{x}(t|t), 0, u(t)) = A_P \hat{x}(t|t) + B_P u(t). \quad (27)$$

To complete the design, relations for  $\zeta, V, A$ , and  $W$ , according to (17), (18), (22), and (23), are found. To begin with  $\zeta$ , consider matrices  $C_1$  and  $C_2$  defined as

$$C_1 = C_{P_1} = [C_{11} \quad C_{12} \quad C_{13} \quad \cdots] \quad (28)$$

$$C_2 = C_{P_2} = [C_{21} \quad C_{22} \quad C_{23} \quad \cdots] \quad (29)$$

where  $C_{1i}$  is the  $i$ th entry of the row vector  $C_1$  and  $C_{2i}$  is the  $i$ th entry of the row vector  $C_2$ . Notice that in this case, a natural partition of the vector state  $x(t)$  is  $\{x_1(t), x_2(t)\}$ , where  $x_1(t)$  and  $x_2(t)$  are the vector states of  $P_1$  and  $P_2$ , respectively. Thus, defining

$$\psi_1(x_1(t)) = C_1 x_1(t), \quad \psi_2(x_2(t)) = C_2 x_2(t) \quad (30)$$

it is immediately clear that

$$\begin{aligned} \phi(t) &= p_1 \psi_1^2(x_1(t)) + p_2 \psi_2^2(x_2(t)) + p_{12} \psi_1(x_1(t)) \psi_2(x_2(t)) \\ &\quad + q_1 \psi_1(x_1(t)) + q_2 \psi_2(x_2(t)) + r + v(t) \end{aligned} \quad (31)$$

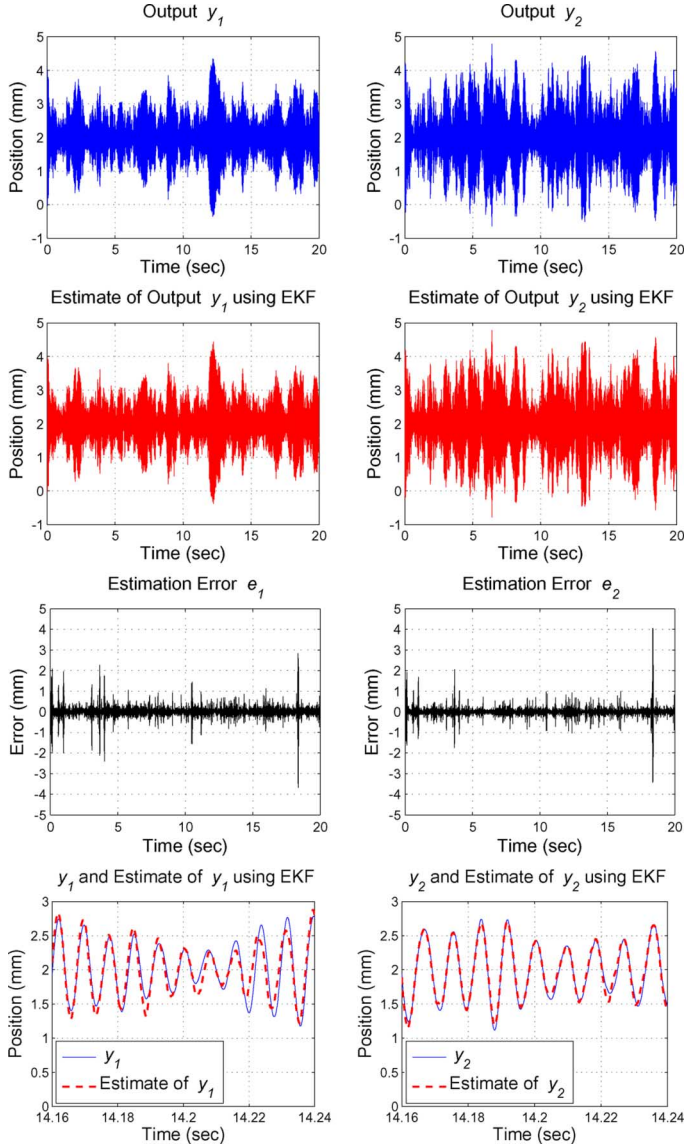


Fig. 6. Open-loop experiment. *Upper Plots:* Output signals  $y_1$  and  $y_2$ . *Plots in the Second Row:* Estimates of outputs signals  $y_1$  and  $y_2$  using the extended Kalman filter method,  $\hat{y}_1$  and  $\hat{y}_2$ , respectively. *Plots in the Third Row:* Estimation errors  $e_1(t) = y_1(t) - \hat{y}_1(t)$  and  $e_2(t) = y_2(t) - \hat{y}_2(t)$ . *Bottom Plots:* Close-ups of plots comparing  $y_1$  with  $\hat{y}_1$  and comparing  $y_2$  with  $\hat{y}_2$ .

and that

$$\frac{\partial \phi}{\partial x_{1i}} = 2p_1 C_{1i} \psi_1 + q_1 C_{1i} + p_{12} C_{1i} \psi_2 \quad (32)$$

$$\frac{\partial \phi}{\partial x_{2i}} = 2p_2 C_{2i} \psi_2 + q_2 C_{2i} + p_{12} C_{2i} \psi_1 \quad (33)$$

which implies that  $\zeta$ , according to (17), is given by

$$\zeta = [\zeta_1 \quad \zeta_2] \quad (34)$$

with

$$\begin{aligned} \zeta_1 &= [2p_1 \psi_1(\hat{x}_1(t|t-1)) + q_1 + p_{12} \psi_2(\hat{x}_1(t|t-1))] C_{P1} \\ \zeta_2 &= [2p_2 \psi_2(\hat{x}_2(t|t-1)) + q_2 + p_{12} \psi_1(\hat{x}_2(t|t-1))] C_{P2}. \end{aligned}$$

Similarly, we obtain

$$V = \Sigma_v, \quad A = A_P, \quad W = B_P \Sigma_{w_P} B_P^T \quad (35)$$

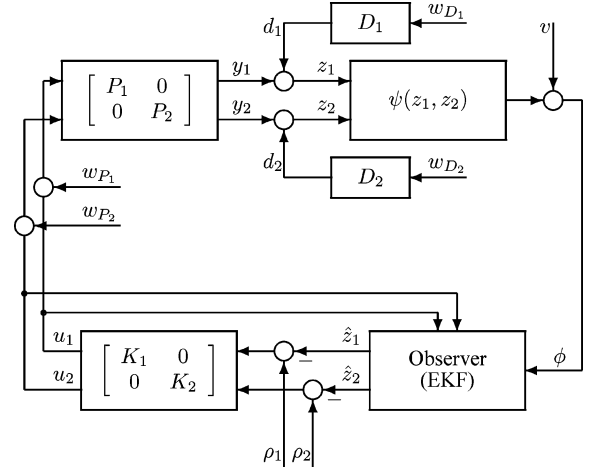


Fig. 7. Signals-and-systems block diagram idealization of the optical system with proposed control scheme.

where  $\Sigma_v = E\{v(t)v^T(t)\}$  and  $\Sigma_{w_P} = E\{w_P(t)w_P^T(t)\}$ , which completes the observer design.

When the EKF algorithm is implemented in the experiment, the states of the physical system are unavailable for measurement. However, a way to test the filter is to input white noise to the open-loop plant and then compare the signals  $y_1$  and  $y_2$ , measured using the OPS, with the estimated signals  $\hat{y}_1 = C_1 \hat{x}_1$  and  $\hat{y}_2 = C_2 \hat{x}_2$ , respectively. Here, and in the rest of the paper,  $\hat{x}_1(t) = \hat{x}_1(t|t-1)$  and  $\hat{x}_2(t) = \hat{x}_2(t|t-1)$ . The results from such experiment are shown in Fig. 6. There, the upper plots show the output signals  $y_1$  and  $y_2$ , the plots in the second row show the estimates  $\hat{y}_1$  and  $\hat{y}_2$ , the plots in the third row show the estimation errors  $e_1(t) = y_1(t) - \hat{y}_1(t)$  and  $e_2(t) = y_2(t) - \hat{y}_2(t)$ , and the bottom plots show close-ups of plots comparing  $y_1$  with  $\hat{y}_1$  and  $y_2$  with  $\hat{y}_2$ . There are two important things to notice in those results. The first one is that the output is biased with respect to  $(0, 0)$  and with respect to  $y^*$ , which is the result of the biased input necessary for the filter to work satisfactorily. The second is that for this kind of input, with significant high frequency content, the filter yields an estimate close to the true signal. This can be clearly seen in the bottom plots. Notice that in some places, as at time  $t = 14.22$  s in the left plot, a small phase shift between the measured and estimated signals appears, which is reflected as spikes in the estimation errors. This phenomenon is explained by the significant high frequency content of the white signals used as inputs, and it does not mean that the real-time estimation process is deficient for control purposes.

## VI. OBSERVER-BASED CONTROLLER DESIGN

The proposed observer-based control scheme is depicted in the idealized block diagram in Fig. 7, which shows the interaction between all the subsystems involved. There,  $P_1$  and  $P_2$  represent the discrete-time open-loop LTI systems corresponding to the Axis 1 and Axis 2 of the actuator microelectromechanical mirror, respectively. The systems  $K_1$  and  $K_2$  are LTI controllers designed under the assumption that  $\hat{z}_1 = z_1$  and  $\hat{z}_2 = z_2$ . The function  $\psi$  is the mapping from the 2-D position of the laser beam spot on the OPS to the noise-free light intensity measurement from the photodiode. The inputs to the observer are the

inputs to  $P_1$  and  $P_2$  and the noisy light intensity measurement  $\phi$ . The outputs from the observer are estimates for the position signals  $z_1$  and  $z_2$ . The output disturbances  $d_1$  and  $d_2$  represent the aggregated effects of all the disturbances injected to the optical system by FSM 2 and possibly by the shaker. Similarly, the signal  $v$  represents the aggregated effects of physical sensor noise in the photodiode and mismatch between the true and idealized mappings  $\psi$ . Finally,  $\rho_1$  and  $\rho_2$  are position references generated inside the digital signal processor.

The observer design assumes the stable LTI disturbance models

$$d_1 = D_1 w_{D_1}, \quad d_2 = D_2 w_{D_2} \quad (36)$$

where  $w_{D_1}$  and  $w_{D_2}$  are stationary zero-mean white random processes. The models  $D_1$  and  $D_2$  can be identified accurately, as in [3], or they can be chosen according to *a priori* information. Notice that the parameters defining the filters  $D_1$  and  $D_2$  will become design parameters of the observer, and therefore, an exact knowledge of  $D_1$  and  $D_2$  will not be needed in practice. Also for purposes of design,  $v$  is assumed to be stationary, zero-mean and white, and the mapping  $\psi$  is considered to be a quadratic function of  $z = d + y$ , i.e.,

$$\psi(z_1, z_2) = p_1 z_1^2 + p_2 z_2^2 + p_{12} z_1 z_2 + q_1 z_1 + q_2 z_2 + r. \quad (37)$$

Thus, considering Fig. 7, (36) and (37) the augmented open-loop nonlinear model to be employed in the design of the observer is given by

$$x(t+1) = f(x(t), w(t), u(t)) = A_\phi x(t) + B_w w(t) + B_u u(t) \quad (38)$$

$$z(t) = \begin{bmatrix} z_1(t) \\ z_2(t) \end{bmatrix} = C_\phi x(t), \quad (39)$$

$$\phi(t) = \psi(z_1(t), z_2(t)) + v(t) \quad (40)$$

where

$$A_\phi = \begin{bmatrix} A_{P_1} & 0 & 0 & 0 \\ 0 & A_{D_1} & 0 & 0 \\ 0 & 0 & A_{P_2} & 0 \\ 0 & 0 & 0 & A_{D_2} \end{bmatrix}$$

$$B_w = B_u = \begin{bmatrix} B_{P_1} & 0 & 0 & 0 \\ 0 & B_{D_1} & 0 & 0 \\ 0 & 0 & B_{P_2} & 0 \\ 0 & 0 & 0 & B_{D_2} \end{bmatrix}$$

$$C_\phi = \begin{bmatrix} C_{P_1} & C_{D_1} & 0 & 0 \\ 0 & 0 & C_{P_2} & C_{D_2} \end{bmatrix}.$$

The sets of matrices  $\{A_{P_1}, B_{P_1}, C_{P_1}\}$ ,  $\{A_{P_2}, B_{P_2}, C_{P_2}\}$ ,  $\{A_{D_1}, B_{D_1}, C_{D_1}\}$ , and  $\{A_{D_2}, B_{D_2}, C_{D_2}\}$  define state-space realizations for the systems  $P_1$ ,  $P_2$ ,  $D_1$ , and  $D_2$ , respectively. The signals  $w(t)$  and  $u(t)$  are formed as

$$w(t) = \begin{bmatrix} w_{P_1}(t) \\ w_{D_1}(t) \\ w_{P_2}(t) \\ w_{D_2}(t) \end{bmatrix}, \quad u(t) = \begin{bmatrix} u_1(t) \\ 0 \\ u_2(t) \\ 0 \end{bmatrix} \quad (41)$$

where  $w_{P_1}$  and  $w_{P_2}$  are stationary zero-mean white random processes, inputs to  $P_1$  and  $P_2$ , respectively. Similar to  $w_{D_1}$  and  $w_{D_2}$ ,  $w_{P_1}$ , and  $w_{P_2}$  are assumed for design purposes, but those

are not necessarily true signals driving the system. The signals  $u_1$  and  $u_2$  are deterministic known signals generated inside the digital signal processor, using controller  $K$ .

Notice that, as in the previous section, since (38) depends on  $u(t)$ , the form of (38) is slightly different from the form of (12). However, this will not modify the EKF design algorithm significantly, because  $u(t)$  is known by the observer. Then, the system state estimate is time-updated as

$$\hat{x}(t+1|t) = f(\hat{x}(t|t), 0, u(t)) = A_\phi \hat{x}(t|t) + B_u u(t). \quad (42)$$

Relations for  $\zeta$ ,  $V$ ,  $A$ , and  $W$  are found according to (17), (18), (22), and (23). Similarly, to the case described in the previous section,  $\zeta$  is computed as follows. First, matrices  $C_1$  and  $C_2$  are formed as

$$C_1 = [C_{P_1} \ C_{D_1}] = [C_{11} \ C_{12} \ C_{13} \ \dots] \quad (43)$$

$$C_2 = [C_{P_2} \ C_{D_2}] = [C_{21} \ C_{22} \ C_{23} \ \dots] \quad (44)$$

where  $C_{1i}$  is the  $i$ th entry of the row vector  $C_1$  and  $C_{2i}$  is the  $i$ th entry of the row vector  $C_2$ . Also, the state-vector is partitioned as

$$x(t) = \begin{bmatrix} x_1(t) \\ x_2(t) \end{bmatrix} \quad (45)$$

according the dimensions of  $C_1$  and  $C_2$ , i.e.,  $x_1(t)$  has the same number of elements as  $C_1$  and  $x_2(t)$  has the same number of elements as  $C_2$ . Notice that in this case,  $x_1(t)$  and  $x_2(t)$  do not correspond to the state vectors of  $P_1$  and  $P_2$ , respectively, as in the open-loop case considered in Section V.

Now, with these definitions in mind, the steps in (30) to (33) can be repeated, which according to (17) yields

$$\zeta = [\zeta_1 \ \zeta_2] \quad (46)$$

with

$$\zeta_1 = [2p_1\psi_1(\hat{x}_1(t|t-1)) + q_1 + p_{12}\psi_2(\hat{x}_1(t|t-1))] C_1$$

$$\zeta_2 = [2p_2\psi_2(\hat{x}_2(t|t-1)) + q_2 + p_{12}\psi_1(\hat{x}_2(t|t-1))] C_2.$$

Also, it can be shown that

$$V = \Sigma_v, \quad A = A_\phi, \quad W = B_w \Sigma_w B_w^T \quad (47)$$

which completes the augmented observer design to be implemented in the closed-loop in Fig. 7. Consistently with the notation in Section V, here

$$\hat{z}(t) = \begin{bmatrix} \hat{z}_1(t) \\ \hat{z}_2(t) \end{bmatrix} = C_\phi \hat{x}(t|t-1). \quad (48)$$

## VII. CLOSED-LOOP EXPERIMENTS

### A. Description of the Experiments

A photodiode is a semiconductor light sensor that generates a current or voltage when its P-N junction is illuminated by light, making possible the detection of intensity of light [11]. In the experiment described here, a HAMAMATSU S6468 photodiode, connected in the basic form, is utilized to generate a voltage related by a linear function with negative slope to intensity of light. Since the slope of the linear relation is negative, when

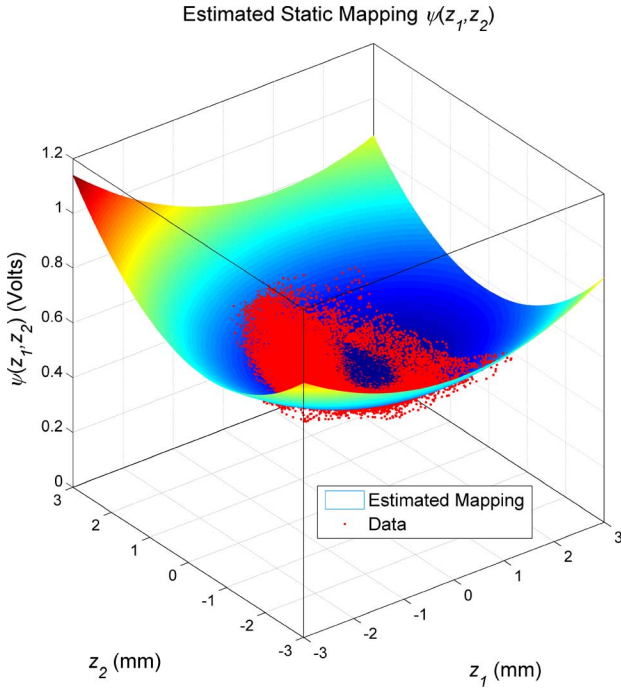


Fig. 8. Estimated static mapping  $\psi(z_1, z_2)$ , computed using the minimum least-squares algorithm, employing 450 000 data samples. The plot also shows some of the data samples used in the estimation.

the light intensity increases the photodiode output voltage decreases. Thus, if no light is incidenting the photodiode sensor surface, the voltage output is a positive number greater than zero. Conversely, if the amount of light illuminating the photodiode sensor surface is too large, the sensor saturates and the voltage output is equal to zero. In the experiments described here, the maximum intensity is measured when the center of the laser-beam spot is centered on the center of the photodiode center. In order for the proposed scheme to work, the maximum measured intensity must correspond to a positive voltage sensor output. Specifically, saturation is intentionally avoided by filtering part of the light incidenting the photodiode sensor. This is achieved simultaneously when the laser beam is split using an Edmund NT47–127 beam splitter, designed for lasers with wavelengths of 632.8 nm, like the one used here. Thus, for the specific configuration described in Section II, the measurement range is  $[0.4470, 0.8157]$  V.

With the previous facts in mind, in this work we ignore the unit transformation, and therefore, the control implementation and the data analysis are conducted using units of voltage. Notice that by using the photodiode sensor voltage output for feedback, the mapping  $\psi$  becomes a convex function, and consequently, the optimal operation point is the closest point in the surface determined by  $\psi$  to the plane  $\{z_1 = 0, z_2 = 0\}$ . An estimate of the mapping  $\psi(z_1, z_2)$  computed using the minimum least-squares method, employing 450 000 data samples, is shown in Fig. 8.

There are some important things to notice about the identified convex mapping  $\psi(z_1, z_2)$ . Having it the form of (37) and being it convex, it follows that the minimizing point  $\{z_1^*, z_2^*\}$  satisfies the conditions

$$\frac{\partial \psi(z_1, z_2)}{\partial z_1} = 2p_1 z_1 + p_{12} z_2 + q_1 = 0 \quad (49)$$

$$\frac{\partial \psi(z_1, z_2)}{\partial z_2} = 2p_2 z_2 + p_{12} z_1 + q_2 = 0. \quad (50)$$

Therefore, it is immediately obvious that

$$\begin{bmatrix} z_1^* \\ z_2^* \end{bmatrix} = - \begin{bmatrix} 2p_1 & p_{12} \\ p_{12} & 2p_2 \end{bmatrix}^{-1} \begin{bmatrix} q_1 \\ q_2 \end{bmatrix}. \quad (51)$$

From that, we define

$$\phi^* = \psi^* = \psi(z_1^*, z_2^*) = \phi(z_1^*, z_2^*, v = 0). \quad (52)$$

In the identified system considered in this paper  $z_1^* = 0.6230$ ,  $z_2^* = -0.1553$ , and  $\phi^* = 0.4586$ . It is important to state that these three values are very important in the experiments presented here. First, notice that if the output from the OPS was exactly  $z_1^*$  and  $z_2^*$ , then theoretically in the absence of sensor noise, for that specific optical configuration the output  $\phi$  from the photodiode sensor would be exactly the minimum possible value  $\phi^*$ , which obviously, in the absence of sensor noise and modeling errors, should coincide with the lower bound of the photodiode sensor output, for the specific configuration considered here. Therefore, two ways of measuring the proposed controller performance naturally emerge: one based on the difference between  $\phi(t)$  and  $\phi^*$ , measured in volts, and another based on the distance from the point  $\{z_1(t), z_2(t)\}$  to the point  $\{z_1^*, z_2^*\}$ , measured in millimeters. For these reasons, in the next subsection the performance indices employed are functions of the variables just described.

Another fact about  $z^*$  is that in all the experiments described here, it was observed that the position  $\{z_1^* = 0.6230, z_2^* = -0.1553\}$  is not achievable using the control scheme proposed in Fig. 7. This is because the observer fails in estimating the laser-spot position when this is exactly over the optimal point  $\{z_1^*, z_2^*\}$ . As shown in the experiments in the next subsection, this issue is resolved by setting references  $\rho_1$  and  $\rho_2$  biased with respect to the optimal point  $z^*$ , in this case  $\{\rho_1(t) = 0, \rho_2(t) = 0\}$ ,  $\forall t$ . Notice that  $\{\rho_1(t) = 0, \rho_2(t) = 0\}$ ,  $\forall t$  does not imply that the signal  $u$  is 0, since  $u$  is the output from the controller  $K$ . It can be speculated that the reason for the observer to fail when  $\rho = z^*$  is that in this case there is a relationship between distinguishing signals and  $z^*$ , similar to what is observed in the open-loop cases of Examples 1 and 2, however this is a matter of further research.

## B. Experimental Results

In this section, we show the results from four experiments, and through them, we explain in which cases the approach proposed here is feasible, and demonstrate its potentials and limitations. An important thing to notice is that the bandwidths of the LTI sensitivity transfer functions in Fig. 3 are approximately 224 and 233 Hz, for channels 1 and 2, respectively. This establishes a hard constraint over the performance of the observer-based controller, since no matter how accurate the estimates of the system states are, the performance achieved by the intensity-based controller could never surpass the LTI performance achievable by the controller  $K$  in Fig. 4, using the biaxial OPSs.

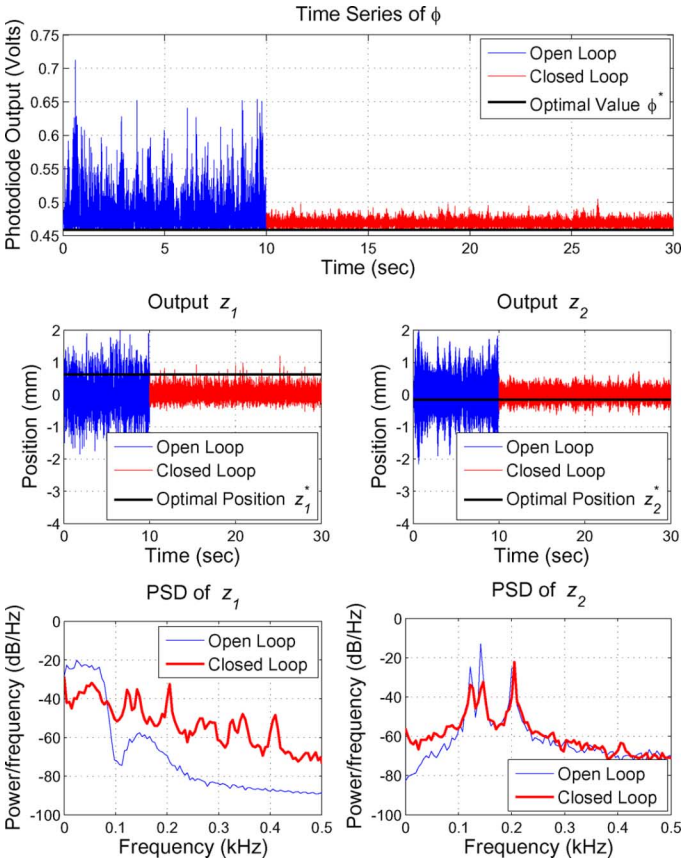


Fig. 9. Closed-loop experimental Case 1. *Upper Plot*: Time series of photodiode output  $\phi$ . *Middle Plot*: Time series of positions signals  $z_1, z_2$ . *Bottom Plot*: PSDs of  $z_1, z_2$ .

In the first case studied (Case 1 in Figs. 9 and 10), the disturbance to channel 1 has a spectrum of wide low-frequency content on the range  $[0, 70]$  Hz. The disturbance inputted to channel 2 has a spectrum composed of three narrowband disturbances. The results show that the proposed control scheme is capable of rejecting disturbances on the range  $[0, 200]$  Hz. The power spectral densities (PSDs) in Fig. 9 demonstrate that in channel 1 the disturbance band is attenuated by 20 dB, and the first two narrow-bands of the disturbance of channel 2 are attenuated by 10 and 20 dB, approximately. The third peak, over 200 Hz, however, is not rejected. This behavior is expected from the shape of the sensitivity functions in Fig. 3.

What is particular to the experiments presented here is that, in closed-loop, the spectrum of channel 2 is projected on the spectrum of channel 1, and in a lesser degree, the spectrum of channel 1 is projected on the spectrum of channel 2. This phenomenon indicates that there exists cross interference introduced by the light-intensity sensor that cannot be completely decoupled by the observer. This implies that there is a fundamental limitation on the achievable performance of the proposed control scheme, because coincidental wide-band disturbances in channels 1 and 2 would interfere with each other, making a significant rejection extremely difficult. This is a matter of further research.

As a direct consequence of the disturbance rejection in each channel, the average value of the photodiode

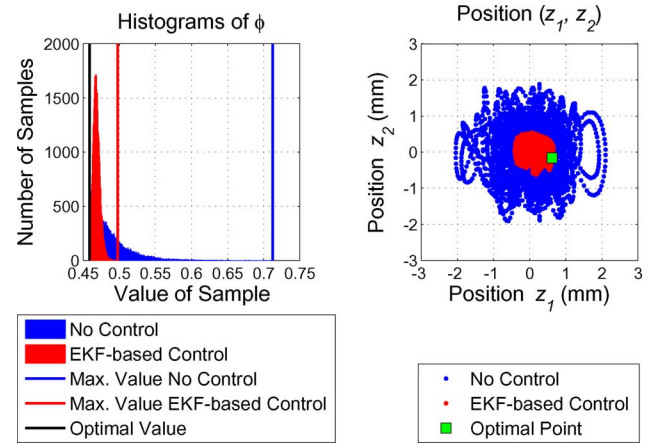


Fig. 10. Closed-loop experimental Case 1. *Left Plot*: Histograms of photodiode output  $\phi$ . The samples are measured in volts. *Right Plot*: 2-D position of the laser-beam spot on the OPS.

output is significantly closer to the optimal value  $\phi^*$ , despite the fact that  $\{\rho_1(t) = 0, \rho_2(t) = 0\}, \forall t$ , and not  $\{\rho_1(t) = z_1^*, \rho_2(t) = z_2^*\}, \forall t$ . This can be observed in the time series of the upper plot in Fig. 9, and in the histogram of Fig. 10. Also in Fig. 10, a 2-D plot shows the position of the center of the laser spot on the OPS,  $\{z_1(t), z_2(t)\}$ , of 4,000 samples, in open-loop (blue) and closed-loop (red). Notice that the attenuation observable in the signal  $\phi$  appears to be more significant than the attenuation in signals  $z_1$  and  $z_2$ . This phenomenon is explained by the shape of the nonlinear mapping  $\psi$ . Notice, that the surface of the paraboloid in Fig. 8 is almost flat around the optimal point  $\{z_1^*, z_2^*\}$ , marked with a green square on the left plot of Fig. 10. Exactly the same comment can be made in reference to Figs. 12, 14, and 16, corresponding to Cases 2, 3, and 4 to be discussed in the following paragraphs.

Case 2 in Figs. 11 and 12 shows that two narrow-banded disturbances, in channels 1 and 2, respectively, on similar frequency ranges, can be effectively rejected. Similarly, Figs. 13 and 14 show Case 3, in which two wide-banded, relative to the bandwidth of the sensitivity function in Fig. 3, disturbances are inputted to channels 1 and 2, respectively. The frequency band of the disturbance in channel 1 is  $[10, 60]$  Hz, and the frequency band of the disturbance in channel 2 is  $[120, 160]$  Hz. Despite being wide-banded, these disturbances can be effectively attenuated. Notice that as in the previous cases, the spectrums of the disturbances inputted to channels 1 and 2 are cross projected onto channels 2 and 1, respectively. Therefore, the significant disturbance rejection is explained by the facts that the corresponding frequency bands are located inside the sensitivity functions' ranges of rejection, and that both bands do not overlap.

In Figs. 15 and 16, we show a case in which the two disturbance sequences inputted to the system have narrow frequency bands that overlap completely on the range  $[180, 190]$  Hz. In real-life implementations, this disturbance profile could be the result of mechanical vibrations, for example. In order to make the experiment more realistic, additionally to the overlapping frequency bands, the rest of the spectrum profile is very similar to the one in Case 3. The results show that the controller

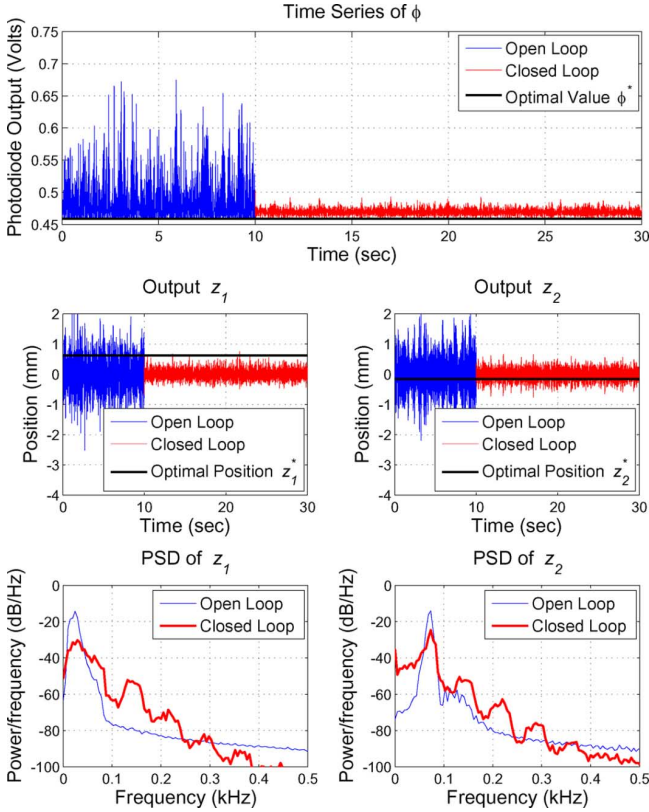


Fig. 11. Closed-loop experimental Case 2. *Upper Plot*: Time series of photodiode output  $\phi$ . *Middle Plot*: Time series of positions signals  $z_1$ ,  $z_2$ . *Bottom Plot*: PSDs of  $z_1$ ,  $z_2$ .

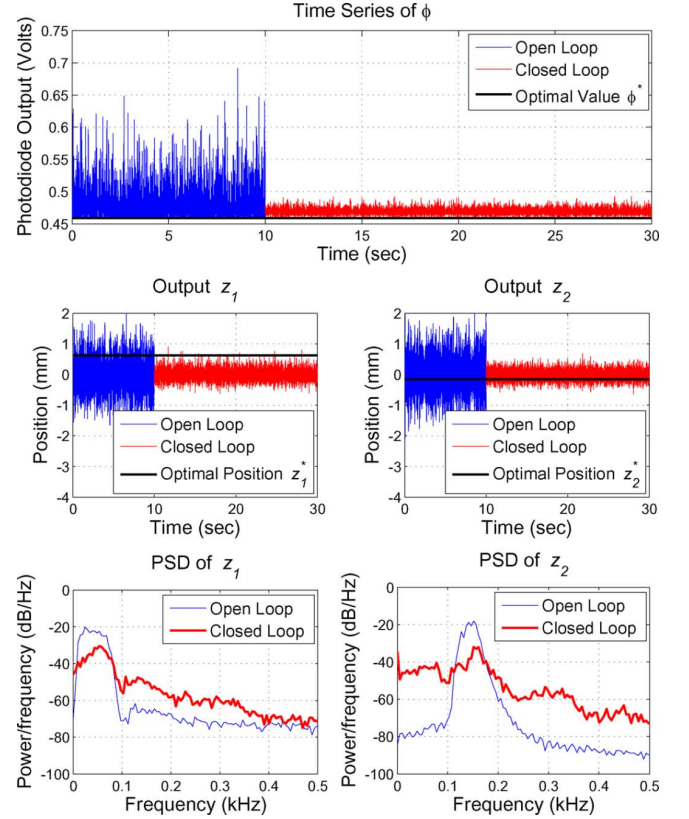


Fig. 13. Closed-loop experimental Case 3. *Upper Plot*: Time series of photodiode output  $\phi$ . *Middle Plot*: Time series of positions signals  $z_1$ ,  $z_2$ . *Bottom Plot*: PSDs of  $z_1$ ,  $z_2$ .

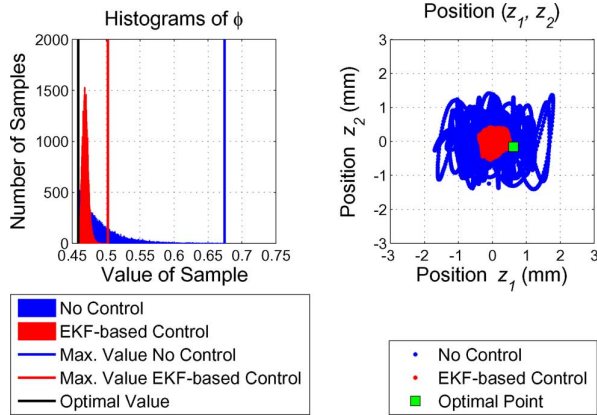


Fig. 12. Closed-loop experimental Case 2. *Left Plot*: Histograms of photodiode output  $\phi$ . The samples are measured in volts. *Right Plot*: 2-D position of the laser-beam spot on the OPS.

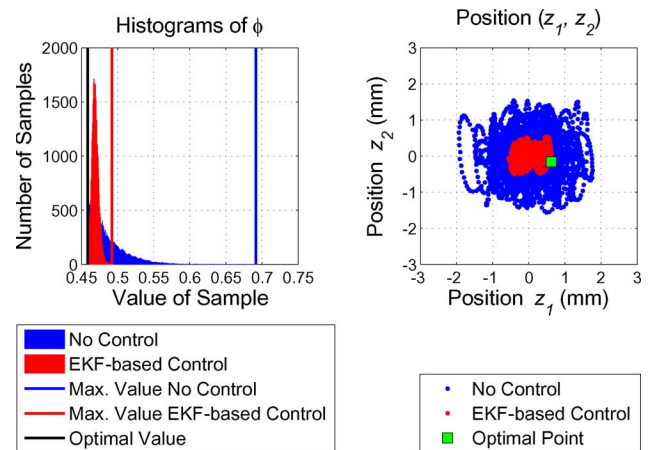


Fig. 14. Closed-loop experimental Case 3. *Left Plot*: Histograms of photodiode output  $\phi$ . The samples are measured in volts. *Right Plot*: 2-D position of the laser-beam spot on the OPS.

scheme is capable of significantly attenuating the disturbances affecting both channels. In this case, what is interesting to notice is that the overlapping frequency bands are noticeably attenuated, however, not as much as in the cases in which the frequency bands do not overlap. This is explained by the cross interference between both channels, already commented in reference to Cases 1, 2, and 3.

Tables I and II summarize the results obtained from the experiments perviously described. The time-series can be evaluated using the empirical standard deviation (*std* in MATLAB), which

are denoted by  $\sigma_{z_1}$ ,  $\sigma_{z_2}$ , and  $\sigma_\phi$ , shown in Table I. However, the standard deviation is not a completely adequate performance index when evaluating the diode output  $\phi$ , because the control objective is to concentrate the laser-beam power on a region of the OPS as small as possible. For this case, we define the index

$$\epsilon_\phi = \frac{\sum_{i=1}^{N_\phi} |\phi(i) - \phi^*|}{N_\phi} \quad (53)$$

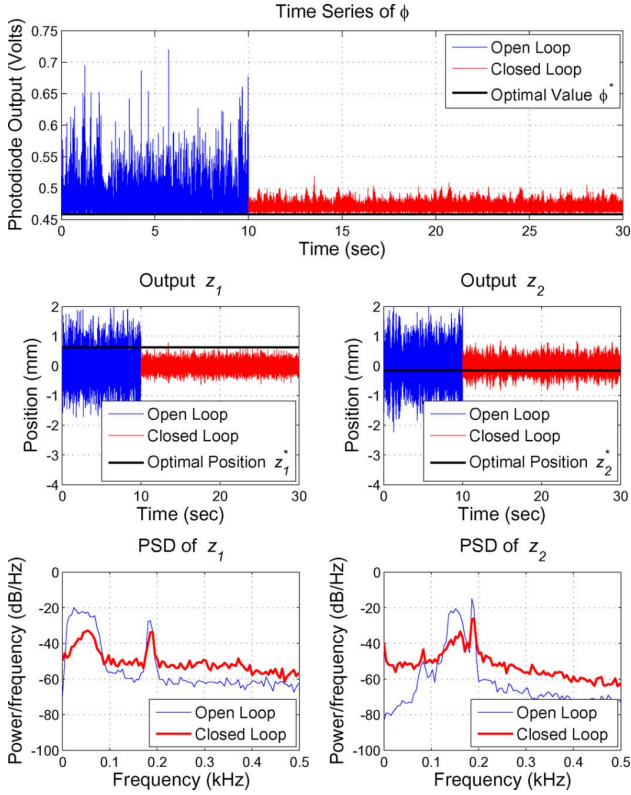


Fig. 15. Closed-loop experimental Case 4. *Upper Plot*: Time series of photodiode output  $\phi$ . *Middle Plot*: Time series of positions signals  $z_1, z_2$ . *Bottom Plot*: PSDs of  $z_1, z_2$ .

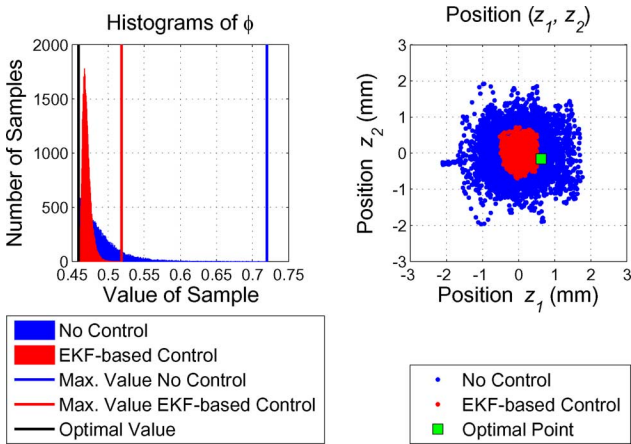


Fig. 16. Closed-loop experimental Case 4. *Left Plot*: Histograms of photodiode output  $\phi$ . The samples are measured in volts. *Right Plot*: 2-D position of the laser-beam spot on the OPS.

where the integer  $N_\phi$  is the length of the sequence  $\phi$  and  $\phi^*$  is the optimal value of the diode output voltage. Notice, that since  $\phi(i) \geq \phi^*, \forall i$ , it follows that

$$\epsilon_\phi = \frac{\sum_{i=1}^{N_\phi} (\phi(i) - \phi^*)}{N_\phi} = \frac{\sum_{i=1}^{N_\phi} \phi(i)}{N_\phi} - \phi^* = \mu_\phi - \phi^* \quad (54)$$

where  $\mu_\phi$  is the empirical mean of the sequence  $\phi$ . Thus, the indices  $\mu_\phi$  and  $\epsilon_\phi$  are absolutely equivalent, because for

TABLE I  
EMPIRICAL STANDARD DEVIATIONS OF EXPERIMENTAL CASES USING 100 000 DATA POINTS, IN OPEN-LOOP (OL) AND IN CLOSED-LOOP (CL)

case	$\sigma_{z_1}$ OL	$\sigma_{z_1}$ CL	$\sigma_{z_2}$ OL	$\sigma_{z_2}$ CL	$\sigma_\phi$ OL	$\sigma_\phi$ CL
1	0.5950	0.1686	0.5473	0.1726	0.0254	0.0049
2	0.6274	0.1578	0.6179	0.1895	0.0294	0.0045
3	0.5521	0.1774	0.5684	0.1512	0.0242	0.0046
4	0.5712	0.1518	0.5784	0.2305	0.0253	0.0058

TABLE II  
VALUES OF INDEX  $\epsilon_\phi$  FOR FOUR EXPERIMENTAL CASES USING 100 000 DATA POINTS, IN OPEN-LOOP (OL) AND IN CLOSED-LOOP (CL), AND VALUES OF  $R_{CL/OL}$  FOR THE SAME FOUR CASES

case	$\epsilon_{\phi_{OL}}$	$\epsilon_{\phi_{CL}}$	$R_{CL/OL} = \epsilon_{\phi_{CL}}/\epsilon_{\phi_{OL}}$
1	0.0266	0.0101	0.3797
2	0.0303	0.0108	0.3564
3	0.0265	0.0105	0.3962
4	0.0273	0.0115	0.4212

a given configuration,  $\phi^*$  remains fixed. However, for analyzing the results,  $\epsilon_\phi$  is more convenient because it takes more meaningful values, considering the measurement range of the photodiode sensor. The values that this index take, in open- and in closed-loop, for the four cases previously described are shown in Table II. Also, with the previous in mind we define

$$R_{CL/OL} = \frac{\epsilon_{\phi_{CL}}}{\epsilon_{\phi_{OL}}} \quad (55)$$

which can be interpreted as the improvement ratio of  $\epsilon_\phi$  due to the use of light-intensity-based feedback control. Obviously,  $\epsilon_{\phi_{CL}}$  and  $\epsilon_{\phi_{OL}}$  are the values of  $\epsilon_\phi$  in closed- and open-loop, respectively. It is important to state that significantly better performances could have been obtained with the use of OPSs for feedback control. For example, see [2] and [3].

The experimental data shown in Figs. 9–16, and Tables I and II allow us to extract some important conclusions. It is obvious that there are innumerable applications in which the proposed approach is adequate. However, we would like to state some of its limitations and issues that are still matter of research. First, as stated before, the scheme in Fig. 7 is heuristic and there is no guarantee that it would be suitable in every case. Specifically, it is important to notice that this scheme depends on the identification of disturbance models  $D_1, D_2$ , and the static mapping  $\psi$ . Then, clearly if the disturbances affecting the system are time-varying, the proposed scheme would fail because the augmented system given by (38)–(40) is directly determined by the statistical information of disturbances  $d_1$  and  $d_2$ . Second, as seen in experimental case 4 (Figs. 15 and 16), the observed cross projection between the PSDs of channels 1 and 2 significantly decreases the achievable performance results, evidenced in the last row of Table II. Third, it has been observed experimentally that tuning the initial conditions of the observer is difficult, in the sense that they should be chosen relatively close to the true values, in order to avoid instability. This phenomenon is consistent with the convergence and stability properties exhibit by EKF-based observers [21]–[25]. Our philosophy is that these current limitations are matter of further research and they do not necessarily imply fundamental limitations of the chosen approach.

## VIII. CONCLUSION

This paper presented an investigation of the issue of steering a laser beam using only light intensity for feedback. Commonly, in order to steer laser beams, which are subjected to dynamic disturbances, biaxial coordinate sensors are required. In field applications, the position of a laser beam spot on an object can be measured, or estimated, using cameras. In optical experimental laboratory setups, the position of laser beam spots are measured using OPSs, like the one described in Section II and references therein. In the investigation presented in this paper, an optical feedback-controlled optical path is designed, in which the signal used for control is light intensity, measured using a single photodiode sensor. The path is actuated using microelectromechanical steering mirrors, and a standard OPS is used for system identification and for signal monitoring, but not for control. The problem that arises from this experiment is of great interest, because its solution has immediate application to optical communications and should have future application to laser surgery. In optical communications applications, typically, OPSs are unavailable for measuring the position of a laser beam on a remote target or receiver, and only an optical intensity or temperature measurement at a fixed location is available for feedback control to regulate the position of the laser. In surgery applications the use of OPSs is impractical, for obvious reasons. In this article, we showed that the resulting optical system can be modeled as a nonlinear Wiener-Hammerstein polynomial system, and then, we proposed an observer-based control scheme. This approach motivated two research lines that were addressed independently in the article. The first explored the issue of multiple-experiment observability of the nonlinear optical system. The second explored the possibility of employing the EKF algorithm as a base for designing an observer for the chosen control scheme. Compelling results on both issues were presented here, through analyses and experiments, respectively. However, it is necessary to state that many issues remain matter of further research. For example, the EKF is a heuristic solution and there is not a direct connection between general notions of observability for nonlinear systems and the algorithm.

## REFERENCES

- [1] M. A. McEver, D. G. Cole, and R. L. Clark, "Adaptive feedback control of optical jitter using  $Q$ -parameterization," *Opt. Eng.*, vol. 43, no. 4, pp. 904–910, Apr. 2004.
- [2] N. O. Pérez Arancibia, N. Chen, S. Gibson, and T.-C. Tsao, "Variable-order adaptive control of a microelectromechanical steering mirror for suppression of laser beam jitter," *Opt. Eng.*, vol. 45, no. 10, pp. 104–112, Oct. 2006.
- [3] N. O. Pérez-Arancibia, J. S. Gibson, and T.-C. Tsao, "Frequency-weighted minimum-variance adaptive control of laser beam jitter," *IEEE/ASME Trans. Mechatron.*, vol. 14, no. 3, pp. 337–348, Jun. 2009.
- [4] T. E. Knibbe, "Spatial tracking using an electro-optic nutator and a single-mode optical fiber," M.S. thesis, Dept. Elect. Eng. Comput. Sci., Massachusetts Inst. Technol., Cambridge, MA, 1993.
- [5] G. L. Plett, "Adaptive inverse control of linear and nonlinear systems using dynamic neural networks," *IEEE Trans. Neural Netw.*, vol. 14, no. 2, pp. 360–376, Mar. 2003.
- [6] K. B. Ariyur and M. Krstić, *Real-Time Optimization by Extremum-Seeking Control*. Hoboken, NJ: Wiley, 2003.

- [7] E. D. Sontag, "On the observability of polynomial systems, I: Finite-time problems," *SIAM J. Control Opt.*, vol. 17, no. 1, pp. 139–151, Jan. 1979.
- [8] D. Nešić, "A note on observability tests for general polynomial and simple Wiener-Hammerstein systems," *Syst. Control Lett.*, vol. 35, no. 4, pp. 219–227, Nov. 1998.
- [9] S. Boyd, "Lecture Notes EE363 – Linear dynamical systems," Stanford Univ., Stanford, CA, 2008. [Online]. Available: <http://www.stanford.edu/class/ee363/>
- [10] T. Kailath, A. H. Sayed, and B. Hassibi, *Linear Estimation*. Upper Saddle River, NJ: Prentice Hall, 2000.
- [11] Hamamatsu Corporation, "Photodiode technical guide," [Online]. Available: <http://sales.hamamatsu.com/assets/html/ssd/si-photodiode/index.htm>
- [12] H. Kwakernaak and R. Sivan, *Linear Optimal Control Systems*. New York: Wiley-Interscience, 1972.
- [13] B. D. O. Anderson and J. B. Moore, *Optimal Control: Linear Quadratic Methods*. Mineola, NY: Dover Publications, 2007.
- [14] R. Koplun and E. D. Sontag, "Linear systems with sign-observations," *SIAM J. Control Opt.*, vol. 31, no. 5, pp. 1245–1266, Sep. 1993.
- [15] D. Cox, J. Little, and D. O'Shea, *Ideals, Varieties, and Algorithms*. New York: Springer, 2007.
- [16] B. Buchberger, "Gröbner bases: A short introduction for systems theorists," in *Proc. Conf. Comput.-Aided Syst. Theory (EUROCAST)*, Feb. 2001, pp. 19–23.
- [17] E. D. Sontag and Y. Rouchaleau, "On discrete-time polynomials systems," *Nonlinear Anal.: Theory, Methods Appl.*, vol. 1, no. 1, pp. 55–64, Jan. 1976.
- [18] C. W. Brown, "QEPCAD—Quantifier elimination by partial cylindrical algebraic decomposition," 2010. [Online]. Available: <http://www.usna.edu/Users/cs/qepcad/B/QEPCAD.html>
- [19] B. Petschel, "Groebner," Mathworks, Natick, MA, 2010. [Online]. Available: <http://www.mathworks.com/matlabcentral/fileexchange/24478-groebner>
- [20] B. D. O. Anderson and J. B. Moore, *Optimal Filtering*. Mineola, NY: Dover Publications, Inc., 2005.
- [21] L. Ljung, "Asymptotic behavior of the extended Kalman filter as a parameter estimator for linear systems," *IEEE Trans. Autom. Control*, vol. 24, no. 1, pp. 36–50, Feb. 1979.
- [22] Y. Song and J. W. Grizzle, "The extended Kalman filter as a local asymptotic observer for discrete-time nonlinear systems," *J. Math. Syst., Estimation, Control*, vol. 5, no. 1, pp. 59–78, 1995.
- [23] P. E. Moraal and J. W. Grizzle, "Observer design for nonlinear systems with discrete-time measurements," *IEEE Trans. Autom. Control*, vol. 40, no. 3, pp. 395–404, Mar. 1995.
- [24] M. Boutayeb, H. Rafaralahy, and M. Darouache, "Convergence analysis of the extended Kalman filter used as an observer for nonlinear deterministic discrete-time systems," *IEEE Trans. Autom. Control*, vol. 42, no. 4, pp. 581–586, Apr. 1997.
- [25] K. Reif, S. Günther, and R. Unbehauen, "Stochastic stability of the discrete-time extended Kalman filter," *IEEE Trans. Autom. Control*, vol. 44, no. 4, pp. 714–728, Apr. 1999.



**Néstor O. Pérez-Arancibia** (S'05–M'08) received the Ingeniero and M.Eng. degrees from the Pontificia Universidad Católica de Chile, Santiago, Chile, in 2000 and the Ph.D. degree from the Mechanical and Aerospace Engineering Department, University of California, Los Angeles (UCLA), in 2007.

From October 2007 to March 2010, he was a Postdoctoral Scholar with the Laser Beam Control Laboratory and also with the Mechatronics and Controls Laboratory, Mechanical and Aerospace Engineering Department, UCLA. During the summer of 2009, he taught the undergraduate class *Introduction to Feedback and Control Systems* and during the winter of 2009 he taught some lectures for the graduate class *Advanced Digital Control for Mechatronic Systems*. Since April 2010, he has been a Postdoctoral Fellow with the Microrobotics Laboratory, Harvard University, Cambridge, MA. His current interests include microrobotics, feedback control, adaptive filtering, adaptive optics, and mechatronics.



**James S. Gibson** (M'08) received the B.S. degree in aerospace engineering, the M.S. degree in engineering mechanics, and the Ph.D. degree in engineering mechanics from The University of Texas at Austin, Austin, in 1970, 1972, and 1975, respectively.

He served on the faculties of the Aerospace Engineering and Engineering Mechanics Department, The University of Texas at Austin and the Engineering Science and Mechanics Department, Virginia Polytechnic Institute and State University.

In 1977, he joined the faculty of the University of California, Los Angeles (UCLA), where he currently is a Professor of Mechanical and Aerospace Engineering. His research interests include control and identification of dynamical systems and adaptive filtering, with applications to identification and control of flexible structures, control of laser beams and adaptive optics, identification and control of micro inertial sensors, control of fluid flow and noise control.

Prof. Gibson has served as an Associate Editor for the *SIAM Journal on Control and Optimization* and for the IEEE TRANSACTIONS ON AUTOMATIC CONTROL.



**Tsu-Chin Tsao** (S'86–M'88–SM'09) received the B.S. degree in engineering from National Taiwan University, Taiwan, in 1981, and the M.S. and Ph.D. degrees in mechanical engineering from The University of California at Berkeley, Berkeley, in 1984 and 1988, respectively.

He served 11 years on the faculty of the Mechanical and Industrial Engineering Department, The University of Illinois at Urbana-Champaign. In 1999, he joined the faculty of the University of California, Los Angeles (UCLA), where he currently is a Professor

with the Mechanical and Aerospace Engineering Department. His research areas include control systems and mechatronics.

Prof. Tsao has been recognized for his research with awards including the *ASME Journal of Dynamic Systems, Measurement, and Control* Best Paper Award for the papers published in the journal in 1994, the Outstanding Young Investigator Award from ASME Dynamic Systems and Control Division, in 1997, and the Hugo S. Shuck Best Paper Award from American Automatic Control Council, in 2002.